

**CHARACTERISATION OF BIOGENIC SILVER  
NANOPARTICLES-*Garcinia atroviridis*  
TOXICOLOGICAL EFFECTS IN NORMAL AND  
CANCER HUMAN LUNG CELLS**

**MUSTHAHIMAH BINTI MUHAMAD**

**UNIVERSITI SAINS MALAYSIA**

**2024**

**CHARACTERISATION OF BIOGENIC SILVER  
NANOPARTICLES-*Garcinia atroviridis*  
TOXICOLOGICAL EFFECTS IN NORMAL AND  
CANCER HUMAN LUNG CELLS**

by

**MUSTHAHIMAH BINTI MUHAMAD**

**Thesis submitted in fulfilment of the requirements  
for the degree of  
Doctor of Philosophy**

**September 2024**

## ACKNOWLEDGEMENT

*In the name of Allah, The Most Gracious and The Most Merciful.*

Praise be to Allah S.W.T., Lord of the universe and selawat to Prophet Muhammad S.A.W., messenger of Allah. I thank Allah for the completion of this project, Alhamdulillah. I gratefully acknowledge the people who helped in the completion of this project. My love and gratitude go to my beloved parents, Muhamad Bin Yaacob and Zakiah Binti Zakaria, as well as my siblings, who patiently supported and understood me while working on this project. I am blessed with and strengthened by their unconditional support and love.

A special thank goes to Dr. Nik Nur Syazni Nik Mohamed Kamal, my project supervisor, for her substantial contribution to the thesis's content. Throughout the course of my work on the project, she had always been there to support and help in every way she could, and offered valuable suggestions and insights that helped the project proceed successfully. I would like to express my gratitude to my co-supervisors, Professor Dr. Azlan Abdul Aziz and Dr. Yazmin Bustamin for their suggestions and comments on this project. I am also extremely grateful to my co-researcher, Dr. Tan Jen Kit from Department of Biochemistry, PPUKM, for facilitating this study on metabolomics.

A note of gratitude is also extended to the Department of Toxicology, Advanced Medical and Dental Institute, as well as the Electron Microscopy Lab, School of Biological Sciences, for providing me with the equipment and materials needed for this project and for their help. I gratefully acknowledge the Universiti Sains Malaysia (USM) for the fellowship under the USM Fellowship Scheme and Majlis Amanah Rakyat (MARA) for financial aid under the Graduate Excellent Programme.

Finally, I am deeply indebted to Nurul Izzati Zulkifli, Fatin Athirah Abdul Aziz, Dr Noor Zafirah Ismail, Dr Hasni Arsad, Dr Nurhidayah Ab. Rahim, Nor Munira Hashim, Dr. Nadhiratul-Farihin Semail, Wan Nuramiera Faznie Wan Eddis Effendy, Sarah Sapuan, Zaleha Md Toha, Dr. Nurdianah Harif Fadzilah, Dr Rohanizah Abdul Rahim and all my friends who lend their helping hands to help in the completion of this project. I express my deepest gratitude and appreciation to each of them. I am fortunate to have worked with such supportive and proficient individuals throughout this project, and I would not have been able to achieve this without their assistance, encouragement, and support.

Jazaakallahu Khairan Kathiiran.

## TABLE OF CONTENTS

<b>ACKNOWLEDGEMENT</b> .....	<b>ii</b>
<b>TABLE OF CONTENTS</b> .....	<b>iv</b>
<b>LIST OF TABLES</b> .....	<b>xiii</b>
<b>LIST OF FIGURES</b> .....	<b>xvii</b>
<b>LIST OF SYMBOLS</b> .....	<b>xxxiii</b>
<b>LIST OF ABBREVIATIONS</b> .....	<b>xxxv</b>
<b>LIST OF APPENDICES</b> .....	<b>xli</b>
<b>ABSTRAK</b> .....	<b>xlii</b>
<b>ABSTRACT</b> .....	<b>xliv</b>
<b>CHAPTER 1 INTRODUCTION</b> .....	<b>1</b>
1.1 Research background .....	1
1.2 Problem statement .....	4
1.3 Objectives of the study .....	5
1.3.1 General objective.....	5
1.3.2 Specific objectives.....	5
<b>CHAPTER 2 LITERATURE REVIEW</b> .....	<b>6</b>
2.1 Lung .....	6
2.1.1 Anatomy, histology, and physiology .....	6
2.1.2 Pathophysiology .....	7
2.1.3 Lung carcinogenesis .....	8
2.2 Cellular Metabolism .....	14
2.2.1 Fundamentals of cell metabolism.....	14
2.2.2 The hallmark of cancer metabolism .....	16
2.3 Silver nanoparticles (AgNPs).....	18
2.3.1 Introduction .....	18

2.3.2	Synthesis of AgNPs.....	19
2.3.3	Significance of physicochemical properties of AgNPs and biomedical applications.....	29
2.4	Toxicological Aspects of AgNPs .....	38
2.4.1	Introduction .....	38
2.4.2	Routes of exposure and biodistribution.....	39
<b>CHAPTER 3 METHODOLOGY.....</b>		<b>43</b>
3.1	Materials and laboratory equipment.....	43
3.1.1	List of chemicals and reagents .....	43
3.1.2	List of consumables and kits .....	46
3.1.3	List of primers .....	47
3.1.4	List of laboratory equipment.....	48
3.2	Experimental design.....	50
3.3	Preparations of plant extract.....	52
3.4	Biosynthesis of silver nanoparticles (AgNPs-GA).....	52
3.5	Preparation of samples .....	53
3.5.1	<i>G. atroviridis</i> aqueous extract (Leaf-GA) stock solution.....	53
3.5.2	AgNPs-GA stock solution.....	54
3.5.3	AgNPs (commercial) stock solution .....	54
3.5.4	AgNO <sub>3</sub> stock solution.....	55
3.5.5	Cisplatin stock solution.....	55
	3.5.5(a) 0.9 % Sodium Chloride (NaCl) .....	55
	3.5.5(b) 0.5 mg/mL (1.67 mM) of Cisplatin .....	56
3.6	Cell culture .....	57
3.6.1	Human cell lines.....	57
3.6.2	Reagents for cell culture work .....	57
	3.6.2(a) Media .....	57
	3.6.2(b) Fetal bovine serum (FBS).....	58

3.6.2(c)	Penicillin Streptomycin (Pen Strep) solution .....	58
3.6.2(d)	Complete cell culture medium.....	59
3.6.2(e)	Cryopreservation medium .....	59
3.6.2(f)	Assay medium .....	60
3.6.2(g)	1X Phosphate buffered solution (PBS).....	60
3.6.2(h)	1X 0.25 % Trypsin-Ethylenediaminetetraacetic acid (0.25 % Trypsin-EDTA) .....	60
3.6.2(i)	0.4 % Trypan blue solution.....	61
3.6.3	Cell culture protocols and conditions.....	61
3.6.3(a)	Cell retrieval from frozen storage.....	61
3.6.3(b)	Sub-culturing of adherent cells.....	62
3.6.3(c)	Cell counting.....	63
3.6.3(d)	Cryopreservation of cells.....	65
3.7	Cell viability assay .....	66
3.7.1	Preparation of MTT solution (5 mg/mL) .....	66
3.7.2	3-(4,5-dimethylthiazol-2-yl)-2,5-diphenyltetrazolium bromide (MTT) assay .....	67
3.7.3	Selectivity index (SI).....	69
3.8	Detection of ROS production by 5-(and-6)-chloromethyl-2',7'-dichlorodihydrofluorescein diacetate, acetyl ester (CM-H2DCFDA) assay..	70
3.8.1	Treatment of cells for ROS assay.....	71
3.8.2	Preparation of ROS reagent.....	71
3.8.3	Protocol of ROS activity .....	72
3.9	DNA Damage Analysis .....	73
3.9.1	Treatment of cells for Alkaline Comet Assay .....	75
3.9.2	Preparation of Alkaline Comet Assay buffer .....	76
3.9.2(a)	Comet LMAgarose .....	76
3.9.2(b)	Lysis solution.....	76

3.9.2(c)	Alkaline Unwinding Solution (pH > 13, 200 mM NaOH, 1 mM EDTA) .....	76
3.9.2(d)	Alkaline electrophoresis solution (pH >13, 200 mM NaOH, 1 mM EDTA) .....	77
3.9.2(e)	TE buffer (10mM Tris-HCl, pH 7.5, 1 mM EDTA).....	77
3.9.2(e)(i)	1 M Tris-HCl, pH 7.5 .....	77
3.9.2(e)(ii)	0.5 EDTA, pH 8.....	77
3.9.2(e)(iii)	TE buffer (10mM Tris-HCl, pH 7.5, 1 mM EDTA) .....	77
3.9.2(f)	SYBR® Gold staining solution .....	78
3.9.3	Protocol of Alkaline Comet Assay.....	78
3.10	Detection of apoptosis by DAPI and Acridine orange (AO) and propidium iodide (PI) double staining .....	80
3.10.1	Treatment of cells for DAPI and AO/PI staining.....	81
3.10.2	Preparation of staining solution.....	81
3.10.2(a)	4 % paraformaldehyde.....	81
3.10.2(b)	70 % ethanol .....	82
3.10.2(c)	10 µg/mL DAPI.....	82
3.10.2(d)	10 µg/mL Acridine Orange/Propidium Iodide (AO/PI) .....	82
3.10.3	Protocol of detection of apoptosis by DAPI and AO/PI staining .....	83
3.11	Measurement of intracellular Ag <sup>+</sup> concentration .....	84
3.11.1	Treatment of cells for ICP-OES analysis .....	86
3.11.2	Preparation for a silver standard solution.....	86
3.11.3	Inductively coupled plasmon optical emission spectroscopy (ICP-OES) .....	87
3.12	Measurement of cellular uptake of AgNPs-GA .....	88
3.12.1	Treatment of cells for cellular uptake of AgNPs-GA .....	89
3.12.2	Transmission electron microscopy (TEM) analysis.....	90

3.12.2(a)	Reagents and chemicals provided by the Microscopy Unit, School of Biological Sciences, USM.....	90
3.12.2(b)	Cell preparation .....	90
3.12.2(c)	Ultramicrotomy.....	92
3.12.2(d)	Staining.....	92
3.12.2(e)	TEM.....	92
3.13	mRNA expression analysis (Quantitative rt-PCR).....	93
3.13.1	Agarose gel electrophoresis .....	94
3.13.1(a)	1X TAE (Tris-acetate-EDTA) buffer .....	94
3.13.1(a)(i)	0.5 M EDTA stock solution (500 mL)....	94
3.13.1(a)(ii)	50X TAE buffer .....	94
3.13.1(a)(iii)	1X TAE buffer.....	94
3.13.1(b)	Ethidium bromide (EtBr).....	94
3.13.1(c)	Agarose gel.....	95
3.13.1(d)	Electrophoresis .....	95
3.13.2	Isolation of total cellular RNA.....	96
3.13.2(a)	RNA extraction.....	96
3.13.2(b)	Determination of RNA concentration and purity .....	97
3.13.2(c)	Determination of RNA integrity.....	98
3.13.3	Reverse transcription of total RNA to cDNA (cDNA synthesis) .....	98
3.13.3(a)	Denaturation of DNA .....	99
3.13.3(b)	Genomic DNA removal (DNase I treatment).....	100
3.13.3(c)	Reverse transcription (cDNA synthesis) .....	100
3.13.4	Primer efficiency (Standard Curve Method).....	101
3.13.5	Comparative CT ( $\Delta\Delta CT$ ) method.....	104
3.14	LCMS based metabolomics .....	106

3.14.1	Sample preparation for the metabolomics study .....	109
3.14.1(a)	Treatment .....	109
3.14.1(b)	Metabolite Extraction .....	109
3.14.2	UHPLC-Orbitrap MS System .....	110
3.14.3	Quality Control.....	111
3.14.4	Data Pre-processing.....	113
3.14.5	Multivariate Analysis .....	114
3.14.6	Metabolites Annotation.....	116
3.14.7	Pathway Annotation .....	117
3.15	Statistical Analysis .....	117
<b>CHAPTER 4 RESULTS.....</b>		<b>118</b>
4.1	Biogenic synthesis and characterisation of AgNPs-GA.....	118
4.2	Effects of AgNPs-GA on Cell Viability and Inhibitory concentration at 50 % (IC <sub>50</sub> ).....	121
4.2.1	Effects of AgNPs-GA and Controls on Cell Viability of A549 cells.....	121
4.2.2	Effects of AgNPs-GA and Controls in BEAS-2B Cells .....	125
4.2.3	Constant IC <sub>50</sub> .....	128
4.2.4	Selectivity Index (SI) .....	131
4.3	Intracellular ROS Levels .....	133
4.4	DNA Damage Activity by Alkaline Single Cell Gel Electrophoresis (Comet Assay).....	135
4.5	Mechanism of Apoptosis.....	142
4.6	Concentration of Intracellular Silver Ion (Ag <sup>+</sup> ) .....	148
4.7	Cellular Uptake of AgNPs-GA .....	150
4.8	mRNA expression of <i>ATM</i> , <i>Ku80</i> , <i>DNA-PKcs</i> and <i>RAD51</i> genes.....	154
4.8.1	RNA purity and integrity.....	154
4.8.2	Primer efficiency of <i>Beta-actin</i> ( <i>β-actin</i> ), <i>ATM</i> , <i>Ku80</i> , <i>DNA-PKcs</i> and <i>RAD51</i> genes by standard curve method .....	155

4.8.3	Analysis of <i>ATM</i> , <i>Ku80</i> , <i>DNA-PKcs</i> and <i>RAD51</i> mRNA expression using Comparative CT ( $\Delta\Delta\text{CT}$ ) formula.....	158
4.9	Analysis of metabolomic data .....	167
4.9.1	Data reliability analysis based on quality control (QC) samples .....	167
4.9.2	Multivariate statistical analysis of the samples .....	170
4.9.2(a)	Principal Component Analysis (PCA).....	170
4.9.2(b)	Orthogonal Partial Least Squares-Discriminant Analysis (OPLS-DA).....	175
4.9.2(b)(i)	Evaluation of Orthogonal Partial Least Squares-Discriminant Analysis (OPLS-DA) in A549 cells treated with AgNPs-GA vs Control.....	176
4.9.2(b)(ii)	Evaluation of Orthogonal Partial Least Squares-Discriminant Analysis (OPLS-DA) in A549 cells treated with Cisplatin vs Control.....	178
4.9.2(b)(iii)	Evaluation of Orthogonal Partial Least Squares-Discriminant Analysis (OPLS-DA) in A549 cells treated with AgNPs-GA+Cisplatin vs Control.....	180
4.9.2(b)(iv)	Evaluation of Orthogonal Partial Least Squares-Discriminant Analysis (OPLS-DA) in BEAS-2B cells treated with AgNPs-GA vs Control .....	182
4.9.2(b)(v)	Evaluation of Orthogonal Partial Least Squares-Discriminant Analysis (OPLS-DA) in BEAS-2B cells treated with Cisplatin vs Control.....	184
4.9.2(b)(vi)	Evaluation of Orthogonal Partial Least Squares-Discriminant Analysis (OPLS-DA) in BEAS-2B cells treated with AgNPs-GA+Cisplatin vs Control.....	186
4.9.3	Identification of Differentially Expressed Metabolites.....	188
4.9.3(a)	Identification of differentially expressed metabolite (DEMs) in A549 cells.....	189
4.9.3(a)(i)	AgNPs-GA vs Control.....	189

	4.9.3(a)(ii) Cisplatin vs Control.....	198
	4.9.3(a)(iii) AgNPs-GA+Cisplatin vs Control .....	206
4.9.3(b)	Identification of differentially expressed metabolites (DEMs) in BEAS-2B cells .....	214
	4.9.3(b)(i) AgNPs-GA vs Control.....	214
	4.9.3(b)(ii) Cisplatin vs Control.....	219
	4.9.3(b)(iii) AgNPs-GA+Cisplatin vs Control .....	225
4.9.4	Metabolic phenotyping and expression.....	233
	4.9.4(a) Hierarchical clustering analysis and identification of metabolites in A549 cells .....	234
	4.9.4(a)(i) AgNPs-GA vs Control.....	234
	4.9.4(a)(ii) Cisplatin vs Control.....	236
	4.9.4(a)(iii) AgNPs-GA+Cisplatin vs Control .....	238
	4.9.4(b) Hierarchical clustering analysis and identification of metabolites in BEAS-2B cells.....	240
	4.9.4(b)(i) AgNPs-GA vs Control.....	240
	4.9.4(b)(ii) Cisplatin vs Control.....	242
	4.9.4(b)(iii) AgNPs-GA+Cisplatin vs Control .....	244
4.9.5	Metabolic pathway analysis .....	246
	4.9.5(a) Metabolic pathway analysis in A549 cells .....	247
	4.9.5(a)(i) AgNPs-GA vs Control.....	247
	4.9.5(a)(ii) Cisplatin vs Control.....	250
	4.9.5(a)(iii) AgNPs-GA+Cisplatin vs Control .....	253
	4.9.5(b) Metabolic pathway analysis in BEAS-2B cells.....	256
	4.9.5(b)(i) AgNPs-GA vs Control.....	256
	4.9.5(b)(ii) Cisplatin vs Control.....	259
	4.9.5(b)(iii) AgNPs-GA+Cisplatin vs Control .....	262
	4.9.5(c) KEGG Pathway Enrichment Analysis of DEMs.....	265

4.9.5(c)(i) AgNPs-GA vs Control in A549 cells .....	265
4.9.5(c)(ii) AgNPs-GA vs Control in BEAS-2B cells	267
4.9.5(c)(iii) Cisplatin vs Control in A549 cells.....	269
4.9.5(c)(iv) Cisplatin vs Control in BEAS-2B cells ...	271
4.9.5(c)(v) AgNPs-GA+Cisplatin in A549 cells .....	273
4.9.5(c)(vi) AgNPs-GA+Cisplatin in BEAS-2B cells	275
<b>CHAPTER 5 DISCUSSIONS .....</b>	<b>277</b>
5.1 Biosynthesis and physicochemical characteristics of silver nanoparticles (AgNPs-GA) mediated <i>G. atroviridis</i> leaves extract .....	277
5.2 Effects of AgNPs-GA, Leaf-GA, AgNO <sub>3</sub> , and chemically synthesised AgNPs (commercial) on cell viability of A549 and BEAS-2B cell lines.....	279
5.3 Effects of AgNPs-GA on reactive oxygen species (ROS) production.....	282
5.4 Effects of AgNPs-GA on DNA damage activity .....	284
5.5 Mechanism effects of AgNPs-GA on the mechanism of apoptosis.....	286
5.6 Intracellular Ag <sup>+</sup> concentration and AgNPs-GA intracellular uptake.....	288
5.7 Effects of AgNPs-GA on the mRNA expression of <i>ATM</i> , <i>Ku80</i> , <i>DNA-PKcs</i> and <i>RAD51</i> in human lung cells.....	291
5.8 Perturbed metabolic pathways .....	300
<b>CHAPTER 6 .....</b>	<b>314</b>
6.1 Conclusions .....	314
6.2 Limitations of study .....	317
6.3 Future recommendations .....	318
<b>REFERENCES.....</b>	<b>320</b>
<b>APPENDICES</b>	
<b>LIST OF PUBLICATIONS</b>	
<b>LIST OF PRESENTATIONS</b>	

## LIST OF TABLES

	<b>Page</b>
Table 2.1	Different methods used on synthesising AgNPs.....25
Table 2.2	Applications of green synthesis AgNPs in pharmaceutical and biomedical field.....31
Table 3.1	List of chemical and reagents.....43
Table 3.2	List of consumables.....46
Table 3.3	List of commercial kits.....47
Table 3.4	List of primers .....47
Table 3.5	List of laboratory equipment.....48
Table 3.6	Components in preparation of DNase I reaction solution..... 100
Table 3.7	Components of reverse transcription solution ..... 101
Table 3.8	ABI PCR thermal Cycler settings to perform reverse transcription reaction..... 101
Table 3.9	Ten-fold serial dilution of the standards and their concentrations... 102
Table 3.10	Components in the Luna Universal qPCR Master Mix protocols and the required total volume for each target gene..... 103
Table 4.1	Summary of the AgNPs-GA, Leaf-GA, AgNO <sub>3</sub> , AgNPs (commercial), and Cisplatin average IC <sub>50</sub> profiles against A549 and BEAS-2B cell lines and the SI ..... 132
Table 4.2	DNA damage induced by AgNPs-GA, Cisplatin, AgNPs-GA+Cisplatin, and H <sub>2</sub> O <sub>2</sub> on A549 and BEAS-2B cells. Statistical analysis was determined using student T-test..... 137
Table 4.3	Purity and concentration of RNA extraction..... 155
Table 4.4	Range of C <sub>T</sub> values for the five serial dilutions of cDNA ..... 156
Table 4.5	Details on standard curve of <i>β-actin</i> , <i>ATM</i> , <i>Ku80</i> , <i>DNA-PKcs</i> and <i>RAD51</i> ..... 156

Table 4.6	Cross validation and permutation test results for Orthogonal Projections to Latent Structures Discriminant Analysis (OPLS-DA) of AgNPs-GA vs control in A549 cells for positive and negative modes.....	177
Table 4.7	Cross validation and permutation test results for Orthogonal Projections to Latent Structures Discriminant Analysis (OPLS-DA) of Cisplatin vs control in A549 cells for positive and negative modes .....	179
Table 4.8	Cross validation and permutation test results for Orthogonal Projections to Latent Structures Discriminant Analysis (OPLS-DA) of AgNPs-GA+Cisplatin vs control in A549 cells for positive and negative modes .....	181
Table 4.9	Cross validation and permutation test results for Orthogonal Projections to Latent Structures Discriminant Analysis (OPLS-DA) of AgNPs-GA vs control in BEAS-2B cells for positive and negative modes.....	183
Table 4.10	Cross validation and permutation test results for Orthogonal Projections to Latent Structures Discriminant Analysis (OPLS-DA) of Cisplatin vs control in BEAS-2B cells for positive and negative modes.....	185
Table 4.11	Cross validation and permutation test results for Orthogonal Projections to Latent Structures Discriminant Analysis (OPLS-DA) of AgNPs-GA+Cisplatin vs control in BEAS-2B cells for positive and negative modes .....	187
Table 4.12	Number of total metabolite features (MFs), the number of differently expressed metabolites (DEMs) and identified DEMs in AgNPs-GA vs control on A549 cells.....	191
Table 4.13	List of annotated DEMs analysed by LCMS system in A549 cells exposed to AgNPs-GA vs control group.....	193

Table 4.14	Number of total metabolite features (MFs), the number of differently expressed metabolites (DEMs) and identified DEMs in Cisplatin vs control on A549 cells .....	200
Table 4.15	List of annotated DEMs analysed by LCMS system in A549 cells exposed to Cisplatin vs control group .....	202
Table 4.16	Number of total metabolite features (MFs), the number of differently expressed metabolites (DEMs) and identified DEMs in AgNPs-GA+Cisplatin vs control on A549 cells .....	208
Table 4.17	List of annotated DEMs analysed by LCMS system in A549 cells exposed to AgNPs-GA+Cisplatin vs control group .....	210
Table 4.18	Number of total metabolite features (MFs), the number of differently expressed metabolites (DEMs) and identified DEMs in AgNPs-GA vs control on BEAS-2B cells.....	215
Table 4.19	List of annotated DEMs analysed by LCMS system in BEAS-2B cells exposed to AgNPs-GA vs control group .....	217
Table 4.20	Number of total metabolite features (MFs), the number of differently expressed metabolites (DEMs) and identified DEMs in Cisplatin vs control on BEAS-2B cells.....	220
Table 4.21	List of annotated DEMs analysed by LCMS system in BEAS-2B cells exposed to Cisplatin vs control group .....	222
Table 4.22	Number of total metabolite features (MFs), the number of differently expressed metabolites (DEMs) and identified DEMs in AgNPs-GA+Cisplatin vs control on BEAS-2B cells.....	227
Table 4.23	List of annotated DEMs analysed by LCMS system in BEAS-2B cells exposed to AgNPs-GA+Cisplatin vs control group.....	229
Table 4.24	Major metabolic pathways and related differentially expressed metabolites (DEMs) for AgNPs-GA vs control in A549 cells analysed by Metaboanalyst 5.0 software .....	249
Table 4.25	Major metabolic pathways and related metabolites for Cisplatin vs control in A549 cells analysed by Metaboanalyst 5.0 software.....	252

Table 4.26	Major metabolic pathways and related metabolites for AgNPs-GA+Cisplatin vs control in A549 cells analysed by Metaboanalyst 5.0 software .....	255
Table 4.27	Major metabolic pathways and related metabolites for AgNPs-GA vs control in BEAS-2B cells analysed by Metaboanalyst 5.0 software .....	258
Table 4.28	Major metabolic pathways and related metabolites for Cisplatin vs control in BEAS-2B cells analysed by Metaboanalyst 5.0 software. ....	261
Table 4.29	Major metabolic pathways and related metabolites for AgNPs-GA+Cisplatin vs control in BEAS-2B cells analysed by Metaboanalyst 5.0 software .....	264

## LIST OF FIGURES

	<b>Page</b>
Figure 2.1	The lower respiratory system displays the relationship between the respiratory bronchioles, alveoli, and terminal bronchioles. Notice that the alveolar pores are connected to the alveoli. As the branch of the airways passes through the alveolar membrane, the smooth muscle fibers in the airways become shorter. Extracted from Homer and Britto, (2014).....6
Figure 2.2	Normal and cancer cells metabolism. (A) Metabolism in a normal cell; increased flux of pyruvate into mitochondria for the generation of ATP; (B) Warburg Effect in the cancer cell; comprised of three main aspects: 1) enhanced glucose uptake 2) increased lactate secretion and 3) decreased oxidative metabolism (adapted from D’Alessandro and Zolla, 2012). ..... 15
Figure 2.3	Cancer metabolism pathways (adapted from Finley et al., 2013); Highly proliferative cancer cell metabolism utilizes numerous pathways to generate energy, nucleotides, lipids, and amino acids. Signalling pathways controlling nutrient uptake and most common oncogenic events (shown in orange), metabolic enzymes (highlighted in red) and metabolites (shown in blue) whose levels, expression, or activity are altered in cancer, including tRNA. .... 17
Figure 2.4	Different approaches to synthesized AgNPs (adapted and from Garg et al., 2022; Hasan et al., 2022).....20
Figure 2.5	General green synthesis of silver nanoparticles (adapted from Alharbi et al., 2022; Ijaz et al., 2022) .....22
Figure 2.6	Representative mechanism for green synthesis of silver nanoparticles (adapted and modified from Alharbi et al., 2022; Garg et al., 2022; Ijaz et al., 2022).....23
Figure 2.7	The diagram represents the biodistribution and toxicity of silver nanoparticles exhibited by different exposure routes.

	Abbreviations: BBB-blood brain barrier; ALT- alanine transaminase; AST- aspartate transaminase; BNP- B-Type Natriuretic Peptide; PAI-1-plasminogen activator inhibitor-1; PT- prothrombin time; aPTT-activated partial thromboplastin time (Adapted and modified from Ferdous and Nemmar, 2020; Y. Li and Cummins, 2020). .....	39
Figure 3.1	Experimental workflow for the mechanism of toxicological effect of AgNPs-GA in human lung cells. ....	51
Figure 3.2	A diagram of a haemocytometer slide. The Cells were stained with trypan blue. Each square has a surface area of 1 mm <sup>2</sup> , and the depth of the chamber is 0.1 mm. Each square of the hemacytometer corresponds to a total volume of 0.1 mm <sup>3</sup> or 10 <sup>-4</sup> cm <sup>3</sup> . Since 1 cm <sup>3</sup> = 1 mL, the subsequent cell concentration per mL can be determined using the formula mentioned in section 3.7.3(c).....	64
Figure 3.3	MTT assay principle .....	66
Figure 3.4	Representative of IC <sub>50</sub> graph.....	68
Figure 3.5	The principle of ROS detection by 5-(and-6)-chloromethyl-2',7'-dichlorodihydrofluorescein diacetate, acetyl ester (CM-H2DCFDA) assay .....	70
Figure 3.6	The principle of the alkaline comet assay (retrieved from manufacturer's protocol).....	74
Figure 3.7	An image of a single comet cell includes the head, tail and tail moment length.....	74
Figure 3.8	The principle of DAPI, AO and PI staining, demonstrated with a fluorescence filter at the appropriate wavelength. The DAPI dye excites UV light (358 nm) and emits blue light (461 nm). AO dye excites blue light (475 nm) and emits green light (535 nm). The PI dye excites green light (535 nm) and emits red light (617 nm) .....	80
Figure 3.9	The principle of ICP-OES analysis for the measurement of silver ion. The sample solution in HNO <sub>3</sub> was subjected to a nebuliser through a pump and aerosolised. The element (small particles) is	

	transported to the plasma using argon gas. Atoms and ions can absorb energy from the heat of an argon plasma to move an electron from the ground state to the excited state. The light emission is detected, and the signal is measured as an intensity .....85
Figure 3.10	The internalisation or uptake of nanoparticles in cells is suggested via membrane-bound structures, mainly lysosomes, through various mechanisms such as diffusion, clathrin and caveolae-mediated endocytosis, phagocytosis, and pinocytosis .....88
Figure 3.11	The AgNPs-GA uptake was assessed through TEM analysis. The principle of TEM analysis includes cell preparation, ultramicrotomy, staining and observation.....89
Figure 3.12	The principle of two-step real-time PCR. The single-stranded RNA (mRNA) is extracted from the cells. The mRNA is converted to cDNA using the cDNA synthesis kit. The cDNA template is used for real-time PCR to respond to the specific target primer sequence. The primer standard curve is conducted to determine the efficiency of the primer before evaluating the actual sample .....93
Figure 3.13	Flowchart of genomic DNA removal and cDNA synthesis (adapted from Toyobo user manual).....99
Figure 3.14	The principal steps of a metabolomics analysis using LCMS in this present study: (A) Sample preparation, metabolite extraction and UHPLC-Orbitrap MS analysis. (B) Mass spectrometry (MS) detection methods are used to identify the metabolites (compound detection). The raw signals are then processed to produce data that can be used for statistical analysis (data pre-processing). The data is then normalised to reduce technical and system bias. In untargeted research, metabolites are identified using spectral data from a database (data processing). Multivariate and univariate statistical evaluations are utilized to determine significantly expressed metabolites (statistical analyses). Finally, the significantly expressed metabolites then undergo pathway analysis to establish a link to the biological context (function analyses). ..... 108

Figure 3.15	QC approach of the untargeted metabolomics study. QC samples were made up of an aliquot of each biological test sample to create a "master mix" or pooled sample. QC samples were run before, during and after analysis to assess system suitability .....	112
Figure 3.16	Workflow for data pre-processing in Thermo Scientific Compound Discover™ 2.0 (CD 2.0) whereby ‘Untargeted Metabolomics Analysis with Statistics’ approach was used followed by database search in mzCloud to annotate the detected unknown compounds..	114
Figure 4.1	Biosynthesis of <i>G. atroviridis</i> : (A) AgNO <sub>3</sub> , (B) Leaf-GA of <i>G. atroviridis</i> leaves, (C) synthesis of AgNPs-GA at 24 hours, (D) synthesis of AgNPs-GA at 48 hours, and (E) synthesis of AgNPs-GA at 72 hours .....	118
Figure 4.2	UV-Visible spectrum of AgNPs-GA synthesis using Leaf-GA: spectrum of (A) AgNO <sub>3</sub> , (B) Leaf-GA, (C) AgNPs-GA at 24 hours, (D) AgNPs-GA at 48 hours, and (E) AgNPs-GA at 72 hours .....	119
Figure 4.3	Line graph for IC <sub>50</sub> value determination of (A) AgNPs-GA, (B) Leaf-GA, (C) AgNO <sub>3</sub> , (D) AgNPs (commercial), and (E) Cisplatin treatments against A549 cells at 24 hours, 48 hours, and 72 hours. Statistical analysis was determined by using Student T Test (a=*p<0.05, b>**p<0.01, c***p<0.001) compared to the untreated cells.....	124
Figure 4.4	Line graph for IC <sub>50</sub> value determination of (A) AgNPs-GA, (B) Leaf-GA, (C) AgNO <sub>3</sub> , (D) AgNPs (commercial), and (E) Cisplatin treatments against BEAS-2B cells at 24 hours, 48 hours, and 72 hours. Statistical analysis was determined by using Student T-Test (a=*p<0.05, b>**p<0.01, c***p<0.001) compared to the untreated cells.....	127
Figure 4.5	Constant IC <sub>50</sub> values of AgNPs-GA (A) and Cisplatin (B) in A549 cells. IC <sub>50</sub> values at different incubation period were plotted for the determination of constant IC <sub>50</sub> values. The curve decreases against incubation period and eventually reaching constant effect after 48 hours’ time point .....	129

Figure 4.6	Constant IC <sub>50</sub> values of AgNPs-GA (A) and Cisplatin (B) in BEAS-2B cells. IC <sub>50</sub> values at different incubation period were plotted for the determination of constant IC <sub>50</sub> values. The curve decreases against incubation period and eventually reaching constant effect after 48 hours' time point ..... 130
Figure 4.7	Measurement of ROS level in AgNPs-GA, Cisplatin, and combination of AgNPs-GA+Cisplatin treated A549 and BEAS-2B cells at 24 hours. DCF fluorescence intensity was expressed in terms of ROS production. Values are expressed as fold change compared to the control (untreated cells). The intensity of the cells in the control group was set to 1. Significance levels are denoted as follows: a = *p < 0.05, b = **p < 0.01, c = ***p < 0.001. .... 134
Figure 4.8	An image of a single of cell comet consist of head, tail, and tail moment length. Extracted from (Collins et al., 2014)..... 135
Figure 4.9	Images of comet (from lymphocytes), stained with DAPI. They represent classes 0-4 as used for visual scoring (Collins, 2004; Kumaravel et al., 2009)..... 136
Figure 4.10	Correlation between the percentage of DNA in the comet tail and visual scoring of human lymphocytes. Classes are defined as follows: Class 0, 1, 2, 3 and 4 (Collins, 2004)..... 136
Figure 4.11	DNA damage of A549 (A) and BEAS-2B (B) cells were observed under fluorescence microscopy at x100 magnification after being induced by AgNPs-GA, Cisplatin, AgNPs-GA+Cislatin, and H <sub>2</sub> O <sub>2</sub> compared to the untreated cells (negative control) ..... 139
Figure 4.12	Representative image of A549 cells. (A) Morphology by inverted microscopy at x100 magnification, (B) DAPI analysis, (C) merged AO/PI staining showing the effect of individual IC <sub>50</sub> doses of AgNPs-GA, Cisplatin, and AgNPs-GA+Cisplatin on A549 cells at 24 hours. Morphological features of apoptosis including membrane blebbing (blue arrows), nuclear chromatin condensation (red arrows), nuclear chromatin fragmentation (orange arrows) are evident. The fluorescent blue in DAPI images

represents nucleus damage. Yellow and orange merged AO/PI images indicate an early and late-stage apoptosis, respectively. Images were captured at x 400 magnification..... 143

Figure 4.13 Representative image of BEAS-2B cells. (A) Morphology by inverted microscopy at x100 magnification, (B) DAPI analysis, (C) merged AO/PI staining showing the effect of individual IC<sub>50</sub> doses of AgNPs-GA, Cisplatin, and AgNPs-GA+Cisplatin on BEAS-2B cells at 24 hours. Morphological features of apoptosis including membrane blebbing (blue arrows), nuclear chromatin condensation (red arrows), nuclear chromatin fragmentation (orange arrows) are evident. The fluorescent blue in DAPI images represents nucleus damage. Yellow and orange merged AO/PI images indicate an early and late-stage apoptosis, respectively. Images were captured at x 400 magnification..... 145

Figure 4.14 Induction of apoptosis in A549 and BEAS-2B cells after 24 hours incubation with untreated, AgNPs-GA, Cisplatin, and combination of AgNPs-GA+Cisplatin. The data were shown as the mean values ± SD for three independent experiments. Statistical analysis was determined by using Student T-Test to compare the treated cells to the untreated cells and to compare the two independent treatment groups. Significance levels are denoted as follows: a = \*p < 0.05, b = \*\*p < 0.01, c = \*\*\*p < 0.001. Comparisons between A549 and BEAS-2B cells are represented by # = AgNPs-GA, ## = Cisplatin, and ### = AgNPs-GA + Cisplatin. 'ns' indicates not significant. .... 147

Figure 4.15 Measurement of intracellular Ag<sup>+</sup> concentration (ppm) in AgNPs-GA, Cisplatin, and AgNPs-GA+Cisplatin treated on A549 and BEAS-2B cells at 24 hours. Statistical analysis was determined by using Student T-Test to compare the treated cells to the untreated cells and to compare the two independent treatment groups. Significance levels are denoted as follows: a = \*p < 0.05, b = \*\*p < 0.01, c = \*\*\*p < 0.001. Comparisons between A549 and BEAS-2B cells are represented by # = AgNPs-GA, ## = Cisplatin, and ### = AgNPs-GA + Cisplatin. 'ns' indicates not significant. .... 149

Figure 4.16 Intracellular localization of AgNPs-GA, Cisplatin and AgNPs-GA+Cisplatin in A549 cells after 24 h, as observed by TEM. Untreated control cells (A) exhibit no notable morphological changes. In AgNPs-GA-treated cells, nanoparticles are primarily found within membrane-bound structures. High-magnification images reveal AgNPs-GA within lysosomes (thick black arrows) (B(i), D(i)). Localization of AgNPs-GA is indicated in the cytoplasm (thin black arrow). Aggregates of AgNPs-GA are highlighted with a thin red arrow (B(i)). Observed cellular changes include nuclear condensation and nuclear membrane dilation (white arrows) (C) and phagosome formation (D). Abbreviations: N: Nucleus; Nu: Nucleolus; C: Cytoplasm; M: Mitochondria; P: Phagosome; L: Lysosomes; V: Vesicles. Magnifications: A: x2500; B: x4000, B(i): x10000; C: x4000, C(i):x8000; D: x5000, D(i): x10000 ..... 151

Figure 4.17 Intracellular localization of AgNPs-GA, Cisplatin and AgNPs-GA+Cisplatin in BEAS-2B cells after 24 h, as observed by TEM. Untreated control cells (A) exhibit no notable morphological changes. In AgNPs-GA-treated cells, nanoparticles are primarily found within membrane-bound structures. High-magnification images reveal AgNPs-GA within lysosomes (thick black arrows) (B(i), D(i)). Localization of AgNPs-GA is indicated in the nucleus (yellow arrow), and mitochondria (thick blue arrow). Observed cellular changes include nuclear condensation and nuclear membrane dilation (white arrows) (D). Abbreviations: N: Nucleus; Nu: Nucleolus; C: Cytoplasm; M: Mitochondria; L: Lysosomes; V: Vesicles. Magnifications: A: x2500; B: x2000, B(i): x6300; C: x2000, C(i):x5000; D: x2000, D(i): x5000 ..... 153

Figure 4.18 Standard curve of (A) *β-actin*, (B) *ATM*, (C) *Ku80*, (D) *DNA-PKcs* and (E) *RAD51* on primer efficiency analysis..... 157

Figure 4.19 A mRNA expression of *ATM* in both A549 and BEAS-2B cells treated with AgNPs-GA, Cisplatin and AgNPs-GA+Cisplatin at 24 hours. The fold-change was calculated as a relative change in *ATM*

mRNA level in comparison to untreated (control). The threshold of untreated (control) expression was equals to 1.0. The mean values  $\pm$  SD from three independent experiments run in triplicates. Statistical significance was assigned to a fold-change based on Student's Independent T-test (SPSS 27.0) to compare the treated cells to the untreated cells and to compare the two independent treatment groups. Significance levels are denoted as follows: a = \*p < 0.05, b = \*\*p < 0.01, c = \*\*\*p < 0.001. Comparisons between A549 and BEAS-2B cells are represented by # = AgNPs-GA, ## = Cisplatin, and ### = AgNPs-GA + Cisplatin. 'ns' indicates not significant..... 160

Figure 4.20 The distribution of QC samples in a PCA scores plot of positive (A) and negative (B) modes. QC samples were clustered together and were almost centrally located in both PCA score plots, indicating high-quality data. The percentage of variance explained by the two PCs was 55.0 % and 44.8 % in positive and negative modes, respectively. In positive mode, the PC 1 explains 33.5% of the variation, and the PC 2 22.5%. In negative modes, the PC1 explains 25.9 % of the variation and 18.9 % variance of PC 2. Abbreviation: A=A549 cells; B=BEAS-2B cells; Number 1, 2, 3, 4= group of samples ..... 169

Figure 4.21 The distribution of samples from different groups in a PCA scores plot for positive (A) and negative (B) modes. This provides a map of how the treatment group relate to each other. The first principal component (PC 1) represents the most variation of the samples, while the second principal component (PC 2) represents the second most. In positive mode, the PC 1 explains 33.2% of the variation, and the PC 2 23.1%. In negative modes, the PC1 explains 27.6 % of the variation and 18.5 % variance of PC 2. A positive correlation was observed when the groups shared similar information (same quadrant). A negative correlation was observed when groups were positioned in opposite quadrants. In positive ion mode, the treatment and control groups showed no significant difference. In

	negative ion mode, there is a significant variance between them. The groups near the plot's centre (0,0) exhibit average properties. The further away from plot origin, the stronger the effect of variables .....	172
Figure 4.22	OPLS-DA outcome for AgNPs-GA vs control in A549 cells. The distribution of samples in the OPLS-DA score plot for AgNPs-GA vs control in positive (A) and negative (B) modes. The permutation test for positive (C) and negative (D) modes .....	177
Figure 4.23	OPLS-DA outcome for Cisplatin vs control in A549 cells. The distribution of samples in the OPLS-DA score plot for Cisplatin vs control in positive (A) and negative (B) modes. The permutation test for positive (C) and negative (D) modes .....	179
Figure 4.24	OPLS-DA outcome for AgNPs-GA+Cisplatin vs control in A549 cells. The distribution of samples in the OPLS-DA score plot for AgNPs-GA+Cisplatin vs control in positive (A) and negative (B) modes. The permutation test for positive (C) and negative (D) modes .....	181
Figure 4.25	OPLS-DA outcome for AgNPs-GA vs control in BEAS-2B cells. The distribution of samples in the OPLS-DA score plot for AgNPs-GA vs control in positive (A) and negative (B) modes. The permutation test for positive (C) and negative (D) modes.....	183
Figure 4.26	OPLS-DA outcome for Cisplatin vs control in BEAS-2B cells. The distribution of samples in the OPLS-DA score plot for Cisplatin vs control in positive (A) and negative (B) modes. The permutation test for positive (C) and negative (D) modes .....	185
Figure 4.27	OPLS-DA outcome for AgNPs-GA+Cisplatin vs control in BEAS-2B cells. The distribution of samples in the OPLS-DA score plot for AgNPs-GA+Cisplatin vs control in positive (A) and negative (B) modes. The permutation test for positive (C) and negative (D) modes .....	187
Figure 4.28	VIP scores of AgNPs-GA vs control in A549 cells for positive (A) and negative (B) ion modes. The left part lists the significant	

	differences between metabolites. The middle part shows the VIP scores, the right heatmap shows the concentration of the metabolites. ....	190
Figure 4.29	VIP scores of Cisplatin vs control in A549 cells for positive (A) and negative (B) ion modes. The left part lists the significant differences between metabolites. The middle part shows the VIP scores, the right heatmap shows the concentration of the metabolites .....	199
Figure 4.30	VIP scores of AgNPs-GA+Cisplatin vs control in A549 cells for positive (A) and negative (B) ion modes. The left part lists the significant differences between metabolites. The middle part shows the VIP scores, the right heatmap shows the concentration of the metabolites .....	207
Figure 4.31	VIP scores of AgNPs-GA+Cisplatin vs control in BEAS-2B cells for positive (A) and negative (B) ion modes. The left part lists the significant differences between metabolites. The middle part shows the VIP scores, the right heatmap shows the concentration of the metabolites .....	226
Figure 4.32	Hierarchical clustering heat-map analysis of identifies metabolites in AgNPs-GA vs control treated A549 cells. The red colour of the tile indicates high abundance, whilst green indicates low abundance. Abbreviations: A=A549 cells; UT= Untreated control group; AG=AgNPs-GA group; 1,2,3,4= Biological replicates.....	235
Figure 4.33	Hierarchical clustering heat-map analysis of identifies metabolites in Cisplatin vs control treated A549 cells. The red colour of the tile indicates high abundance, whilst green indicates low abundance. Abbreviations: A=A549 cells; UT= Untreated control group; CIS=Cisplatin group; 1,2,3,4= Biological replicates .....	237
Figure 4.34	Hierarchical clustering heat-map analysis of identifies metabolites in AgNPs-GA+Cisplatin vs control treated A549 cells. The red colour of the tile indicates high abundance, whilst green indicates low abundance. Abbreviations: A=A549 cells; UT= Untreated	

	control group; CIS=Cisplatin group; 1,2,3,4= Biological replicates .....	239
Figure 4.35	Hierarchical clustering heat-map analysis of identifies metabolites in AgNPs-GA vs control treated BEAS-2B cells. The red colour of the tile indicates high abundance, whilst green indicates low abundance. Abbreviations: B=BEAS-2B cells; UT= Untreated control group; AG=AgNPs-GA group; 1,2,3,4= Biological replicates .....	241
Figure 4.36	Hierarchical clustering heat-map analysis of identifies metabolites in Cisplatin vs control treated BEAS-2B cells. The red colour of the tile indicates high abundance, whilst green indicates low abundance. Abbreviations: B=BEAS-2B cells; UT= Untreated control group; AG=AgNPs-GA group; 1,2,3,4= Biological replicates .....	243
Figure 4.37	Hierarchical clustering heat-map analysis of identifies metabolites in AgNPs-GA vs control treated BEAS-2B cells. The red colour of the tile indicates high abundance, whilst green indicates low abundance. Abbreviations: B=BEAS-2B cells; UT= Untreated control group; AG=AgNPs-GA group; 1,2,3,4= Biological replicates .....	245
Figure 4.38	Overview of pathway analysis showed altered metabolic pathways for AgNPs-GA vs control in A549 cells. The significant and impactful pathways from the groups comparison were marked with (*) and written in bold letters. X-axis represents the Pathway impact obtained by the out-degree centrality algorithm. The size of the point is related to the pathway impact. Y-axis represents the negative algorithm of the p-value (-log(p)) obtained by the pathway enrichment analysis (-log1.3=0.5; -log2=0.01; -log3=0.001; -log4=0.0001). .....	248
Figure 4.39	Overview of pathway analysis showed altered metabolic pathways for Cisplatin vs control in A549 cells. Affected pathways present in both treatment groups comparisons were marked with (*) and	

written in bold letters. X-axis represents the Pathway impact obtained by the out-degree centrality algorithm. The size of the point is related to the pathway impact. Y-axis represents the negative algorithm of the p-value (-log(p)) obtained by the pathway enrichment analysis (-log1.3=0.5; -log2=0.01; -log3=0.001; -log4=0.0001) .....251

Figure 4.40 Overview of pathway analysis showed altered metabolic pathways for AgNPs-GA+Cisplatin vs control in A549 cells. Affected pathways present in both treatment groups comparisons were marked with (\*) and written in bold letters. X-axis represents the Pathway impact obtained by the out-degree centrality algorithm. The size of the point is related to the pathway impact. Y-axis represents the negative algorithm of the p-value (-log(p)) obtained by the pathway enrichment analysis (-log1.3=0.5; -log2=0.01; -log3=0.001; -log4=0.0001) .....254

Figure 4.41 Overview of pathway analysis showed altered metabolic pathways for AgNPs-GA vs control in BEAS-2B cells. Affected pathways present in both treatment groups comparisons were marked with (\*) and written in bold letters. X-axis represents the Pathway impact obtained by the out-degree centrality algorithm. The size of the point is related to the pathway impact. Y-axis represents the negative algorithm of the p-value (-log(p)) obtained by the pathway enrichment analysis (-log1.3=0.5; -log2=0.01; -log3=0.001; -log4=0.0001) .....257

Figure 4.42 Overview of pathway analysis showed altered metabolic pathways for Cisplatin vs control in BEAS-2B cells. Affected pathways present in both treatment groups comparisons were marked with (\*) and written in bold letters. X-axis represents the Pathway impact obtained by the out-degree centrality algorithm. The size of the point is related to the pathway impact. Y-axis represents the negative algorithm of the p-value (-log(p)) obtained by the pathway enrichment analysis (-log1.3=0.5; -log2=0.01; -log3=0.001; -log4=0.0001) .....260

- Figure 4.43 Overview of pathway analysis showed altered metabolic pathways for AgNPs-GA+Cisplatin vs control in BEAS-2B cells. Affected pathways present in both treatment groups comparisons were marked with (\*) and written in bold letters. X-axis represents the Pathway impact obtained by the out-degree centrality algorithm. The size of the point is related to the pathway impact. Y-axis represents the negative algorithm of the p-value (-log(p)) obtained by the pathway enrichment analysis (-log1.3=0.5; -log2=0.01; -log3=0.001; -log4=0.0001) .....263
- Figure 4.44 Overview of the proposed perturbations in metabolic pathways in A549 cells exposed to AgNPs-GA in respective to the untreated control group for 24 hours. The differentially expressed metabolites (DEMs) are highlighted in bold text. DEMs are present in blue block arrow. The up and down block arrow represent upregulated and downregulated, respectively. UDP-Gal: Uridine 5'-diphosphogalactose; UDP-N-GlcNAc:UDP-N-acetylglucosamine; NAD<sup>+</sup>: Nicotinamide adenine dinucleotide; CMP: Cytidine monophosphate; AMP: Adenosine 5'-monophosphate; IMP: Inosine 5'-monophosphate; GMP: Guanosine monophosphate; ADP: Adenosine diphosphate.....266
- Figure 4.45 Overview of the proposed perturbations in metabolic pathways in BEAS-2B cells exposed to AgNPs-GA in respective to the untreated control group for 24 hours. The differentially expressed metabolites (DEMs) are highlighted in bold text. DEMs are present in yellow block arrow. The up and down block arrow represent upregulated and downregulated, respectively. UDP-Gal: Uridine 5'-diphosphogalactose; UDP-N-GlcNAc:UDP-N-acetylglucosamine; NAD<sup>+</sup>: Nicotinamide adenine dinucleotide; CMP: Cytidine monophosphate; AMP: Adenosine 5'-monophosphate; IMP: Inosine 5'-monophosphate; GMP: Guanosine monophosphate; ADP: Adenosine diphosphate.....268
- Figure 4.46 Overview of the proposed perturbations in metabolic pathways in A549 cells exposed to Cisplatin in respective to the untreated

control group for 24 hours. The differentially expressed metabolites (DEMs) are highlighted in bold text. DEMs are present in blue block arrow. The up and down block arrow represent upregulated and downregulated, respectively. UDP-Gal: Uridine 5'-diphosphogalactose; UDP-N-GlcNAc:UDP-N-acetylglucosamine; NAD<sup>+</sup>: Nicotinamide adenine dinucleotide; CMP: Cytidine monophosphate; AMP: Adenosine 5'-monophosphate; IMP: Inosine 5'-monophosphate; GMP: Guanosine monophosphate; ADP: Adenosine diphosphate.....270

Figure 4.47 Overview of the proposed perturbations in metabolic pathways in BEAS-2B cells exposed to Cisplatin in respective to the untreated control group for 24 hours. The differentially expressed metabolites (DEMs) are highlighted in bold text. DEMs are present in yellow block arrow. The up and down block arrow represent upregulated and downregulated, respectively. UDP-Gal: Uridine 5'-diphosphogalactose; UDP-N-GlcNAc:UDP-N-acetylglucosamine; NAD<sup>+</sup>: Nicotinamide adenine dinucleotide; CMP: Cytidine monophosphate; AMP: Adenosine 5'-monophosphate; IMP: Inosine 5'-monophosphate; GMP: Guanosine monophosphate; ADP: Adenosine diphosphate.....272

Figure 4.48 Overview of the proposed perturbations in metabolic pathways in A549 cells exposed to AgNPs-GA+Cisplatin in respective to the untreated control group for 24 hours. The differentially expressed metabolites (DEMs) are highlighted in bold text. DEMs are present in blue block arrow. The up and down block arrow represent upregulated and downregulated, respectively.UDP-Gal: Uridine 5'-diphosphogalactose; UDP-N-GlcNAc:UDP-N-acetylglucosamine; NAD<sup>+</sup>: Nicotinamide adenine dinucleotide; CMP: Cytidine monophosphate; AMP: Adenosine 5'-monophosphate; IMP: Inosine 5'-monophosphate; GMP: Guanosine monophosphate; ADP: Adenosine diphosphate.....274

Figure 4.49 Overview of the proposed perturbations in metabolic pathways in BEAS-2B cells exposed to AgNPs-GA+Cisplatin in respective to

the untreated control group for 24 hours. The differentially expressed metabolites (DEMs) are highlighted in bold text. DEMs are present in yellow block arrow. The up and down block arrow represent upregulated and downregulated, respectively. UDP-Gal: Uridine 5'-diphosphogalactose; UDP-N-GlcNAc:UDP-N-acetylglucosamine; NAD<sup>+</sup>: Nicotinamide adenine dinucleotide; CMP: Cytidine monophosphate; AMP: Adenosine 5'-monophosphate; IMP: Inosine 5'-monophosphate; GMP: Guanosine monophosphate; ADP: Adenosine diphosphate.....276

Figure 5.1 The schematic diagram provided reveals the effects of AgNPs-GA, Cisplatin and AgNPs-GA+Cisplatin in the respective to the control on the expression level of DNA damage and repair genes in A549 (A) and BEAS-2B (B) cells. The targeted genes are highlighted in bold text. AgNPs-GA, Cisplatin and AgNPs-GA+Cisplatin are present in black, red and purple block arrow, respectively. The up and down block arrow represent upregulated and downregulated, respectively .....292

Figure 5.2 Schematic illustrations of several main metabolic pathways (inner circle) and several main building materials or metabolites that were modulated in A549 and BEAS-2B cells following AgNPs-GA exposure. NAD<sup>+</sup>, oxidized form of nicotinamide adenine dinucleotide; AMP, adenosine monophosphate.....302

Figure 5.3 Schematic illustrations of catabolism of purine nucleosides. Xanthine is the metabolite that can be found in the last two steps of purine catabolism. Xanthine oxidoreductase (XOR) is the rate-limiting enzyme that controls the last two steps of purine catabolism by converting hypoxanthine to xanthine and xanthine to uric acid. IMPDH inosine monophosphate dehydrogenase, ADSL adenylosuccinate lyase, ADSS adenylosuccinate synthase, GMPS guanine monophosphate, cN-I cytosolic 5'-nucleotidase, cN-II cytosolic 5'-nucleotidase II, ADA adenosine deaminase, GDA guanine deaminase, PNP purine nucleoside phosphorylase (the above diagram is adapted from Chen and Meng, (2022)).....309

Figure 5.4 Schematic diagram of the proposed mechanism of AgNPs-GA toxicity based on the experimental data obtained in this study. Magnified metabolic alteration is presented below. Blue arrow represents A549 cells, yellow arrow represents BEAS-2B cells .....313

## LIST OF SYMBOLS

%	Percent
x	Absolute value of x
<	Less than
>	Greater than
≥	Greater than or equal to
μ/L	Microliter
μg Ag/L	Microgram silver per liter
μg/g	Microgram per gram
μg/ml	Microgram per milliliter
AU	Arbitrary unit
g	Gram
h/hr	Hours
M	Molar
m/z	Mass to charge ratio
mA	Miliampere
mg/kg	Milligram per kilogram
mg/L	Milligram per liter
mg/mL	Milligram per milimeter
min	Minute
mL	Mililiter
mm	Milimeter
ms	Miliseconds
MΩcm	Million ohm-centrimeter
ng	Nanogram
nm	Nanometer

° C	Celcius
ppm	Parts per million
rpm	Revolutions per minute
s	Seconds
V	Voltage
v/v	Volume by volume
X g	Gravity
µg/L	Microgram per liter
µm	Micrometer

## LIST OF ABBREVIATIONS

3AMP	Adenosine 5'-monophosphate
A431	Skin Squamous Cell Carcinoma cell line
AAS	Atomic absorption spectrometry
ADP	Adenosine diphosphate
AFM	Atomic force microscopy
Ag	Silver
Ag <sup>+</sup>	Silver ion
Ag <sup>0</sup>	Reduced silver ion
AgNO <sub>3</sub>	Silver nitrate
AgNPs	Silver nanoparticles
ALT	Alanine transaminase
AMPK	Adenosine monophosphate-activated protein kinase
AO	Acridine Orange
aPTT	Activated partial thromboplastin time
AR	Analytical Reagent
AST	Aspartate transaminase
ATM	Ataxia-Telangiectasia Mutated
ATP	Adenosine triphosphate
AuNPs	Gold nanoparticles
β-actin	Beta-actin
Bax	Bcl-2 Associated X-protein
BBB	Blood brain barrier
BEAS-2B	Bronchial epithelial cell line
BET	Brunauer-Emmett-Teller surface area analysis
BG	Bone grafts
BNP	B-Type Natriuretic Peptide
BP	Benzo[a]pyrene
BRAF	B-Raf proto-oncogene
cDNA	Complementary DNA
CF	Cystic fibrosis
Cit	Citrate

CM-H2DCFDA	5-(and-6)-chloromethyl-2',7'-dichlorodihydrofluorescein diacetate, acetyl ester
CMP	Cytidine monophosphate
COPD	Chronic obstructive pulmonary disorder
C <sub>t</sub>	Cycle threshold
CV	Cross-validation
Cys-Gly	Cysteinylglycine
DAPI	4',6-diamidino-2-phenylindole
DBA	Dibenzo[a,h]anthracene
DCF	Dichlorodihydrofluorescein
dCTP	Deoxycytidine triphosphate
DDP	Cisplatin
DDR	DNA damage response
DEMs	Differentially expressed metabolites
DLS	Dynamic light scattering
DMEM	Dulbecco's Modified Eagle's Medium
DMEM - F12	Dulbecco's Modified Eagle's Medium and Ham's F-12
DMSO	Dimethyl sulfoxide
DNA	Deoxyribonucleic acid
DNA-PKcs	DNA-dependent protein kinase
DN Master Mix	DNA Master Mix
DSBs	Double-strand breaks
<i>E.coli</i>	<i>Escherichia coli</i>
EDTA	Ethylenediaminetetraacetic acid
EDX/EDS	Energy dispersive X-ray spectroscopy/ Energy dispersive spectroscopy
ERBB2	Erb-B2 receptor tyrosine kinase-2
ESI	Electrospray ionization mass spectrometry
EtBr	Ethidium Bromide
etc	And other things/and so forth
F	Forward primer
FBS	Fetal bovine serum
FC	Fold change
FDR	False discovery rate
FESEM	Field emission scanning electron microscopy

FEV1	Forced expiratory volume
FMN	Flavin mononucleotide
FTIR	Fourier transform infrared spectroscopy
FVC	Force vital capacity
G0	Resting state/gap state
G1	Growth 1 phase (first growth)
G2	Growth 2 phase (growth and preparation for mitosis)
GCMS	Gas chromatography mass spectrometry
gDNA	Genomic DNA
GMP	Guanosine monophosphate
GOR	Gastro oesophageal reflux
GSH	L-glutathione reduced
GSSG	L-Glutathione oxidized
H <sub>2</sub> O <sub>2</sub>	Hydrogen peroxide
HaCaT	Human keratinocyte cell line
HCC	Hepatocellular carcinoma
HEI-OC1	Cochlear cells
HepG2	Human liver cancer cell line
HER2	Human epidermal growth factor receptor-2
HIV	Human immunodeficiency virus
HMDB	Human Metabolome Database
HNO <sub>3</sub>	Nitric acid
HPLC	High Performance Liquid Chromatography
HPV	Human papillomavirus
HR	Homologous recombination
HRSEM	High resolution scanning electron microscopy
HRTEM	High resolution transmission electron microscopy
i.e	That is/in other words
IC <sub>50</sub>	Inhibitory concentration
ICP-OES	Inductively Coupled Plasma Optical Emission spectroscopy
ID	Identification
IMP	Inosine-5'-monophosphate
KEGG	Kyoto Encyclopaedia of Genes and Genomes
K-RAS	Kirsten rat sarcoma virus

Ku 80	Dimeric protein complex
Ku70/Ku80	Heterodimer
LCMS	Liquid chromatography mass spectrometry
LFTS	Lateral flow test strips
LOAEL	Lowest-observed-adverse-effect level
m/w	Molecular weight
MC	3-methylcholanthrene
MCF-10A	Human breast normal cell line
MCF-7	Human breast cancer cell line
MCF-7/TAMR-1	Human breast cancer/ tamoxifen-resistant cell line
MFs	Metabolites features
mRNA	Messenger RNA
MTT	3-(4,5-dimethylthiazol-2-yl)-2,5-diphenyltetrazolium bromide
MYC	myelocytomatosis oncogene/MYC proto-oncogene protein
NaCl	Sodium chloride
NAD <sup>+</sup>	Nicotinamide adenine dinucleotide
NADH	Nicotinamide adenine dinucleotide + Hydrogen
NADP <sup>+</sup>	Nicotinamide adenine dinucleotide phosphate
NADPH	Nicotinamide adenine dinucleotide phosphate
NaOH	Sodium hydroxide
NCFB	Non-cystic fibrosis bronchiectasis
NHEJ	Non-homologous end joining
NMR	Nuclear Magnetic Resonance
NPs	Nanoparticles
NSCLC	Non-small cell lung cancer
OPLSDA	Orthogonal Projections to Latent Structures Discriminant Analysis
OTM	Olive tail moment
OXPHOS	Oxidative phosphorylation
p(corr)	Correlation
p[1]	Covariance
p53	Tumor protein P53
PAHs	Polycyclic aromatic hydrocarbons
PAI-1	Plasminogen activator inhibitor-1
PARP	Poly (ADP-ribose) polymerase

PBS	Phosphate Buffer Saline
PC1	First principal component
PC2	Second principal component
PCA	Principal Component Analysis
PCR	Polymerase chain reaction
PCs	Principal components
PDI	Polydispersity index
PD-L1	Programmed cell death ligand-1
PenStrep	Penicillin-streptomycin
PI	Propidium Iodide
PI3k/Akt	Phosphatidylinositol 3-kinase/ protein kinase B
PL	Photoluminescence spectroscopy
PLSDA	Partial least squares-discriminant analysis
PPP	Pentose phosphate pathway
PS	Particle sizer
PT	prothrombin time
<i>p</i> -value	Probability value
PVP	Polyvinylpyrrolidone
Q <sup>2</sup>	Goodness of prediction
QC	Quality control
qPCR	Quantitative or Real-time polymerase chain reaction
R	Reverse primer
R <sup>2</sup> / R <sup>2</sup> Y	Goodness of fitness and accuracy
RAD51	RAD51 Recombinase, protein coding gene
RNA	Ribonucleic acid
ROS	Reactive oxygen species
RT	Reverse transcriptase
RT	Retention time
SAED	Selected area electron diffraction pattern
SARS	Severe acute respiratory syndrome
SARS-COV-2	Severe acute respiratory syndrome coronavirus 2
SCC	Squamous cell carcinoma
SCGE	Single Cell Gel Electrophoresis
SCLC	Small-cell lung cancer

SEM	Scanning electron microscopy
SI	Selectivity index
SNPs	Single-nucleotide polymorphic variants
SSBs	Single-strand breaks
STEM	Scanning transmission electron microscopy
TAE	Tris-acetate-EDTA
TB	Tuberculosis
TCA	Tricarboxylic acid cycle
TEM	Transmission electron microscopy
TGA	Thermogravimetric analyzer
THD	Thioridazine
TME	Tumour microenvironment
UDP-Gal	Uridine 5'-diphosphogalactose
UDP-N-GlcNAc	UDP-N-acetylglucosamine
UHPLC	Ultra-High-Performance Liquid Chromatography
UT	Untreated group control
UV-Vis	Ultraviolet visible spectroscopy
VIP	Variable Importance in Projection
vs	Against
XOR	Xanthine oxidoreductase
XRCC1	X-ray repair cross-complementing protein 1
Xrcc5	Ku80
Xrcc6	Ku70
XRD	X-ray diffraction
XRF	X-ray fluorescence
ZP	Zeta potential
$\alpha$ -KG	$\alpha$ -ketoglutarate
$\Delta\Delta C_T$	Comparative CT

## LIST OF APPENDICES

- |            |   |
|------------|---|
| Appendix A | Plate layout of real-time PCR   |
| Appendix B | The gel electrophoresis image   |
| Appendix C | The amplification plot and melt curve of primer efficiency analysis   |
| Appendix D | Details on annotated DEMs in A549 and BEAS-2B cells   |
| Appendix E | Overview of biochemical metabolites involved in major enriched metabolic pathways in A549 and BEAS-2B cells |

**PENCIRIAN KESAN TOKSIKOLOGI NANOPARTIKEL PERAK  
BIOGENIK-GARCINIA ATROVIRIDIS DI DALAM SEL PARU-PARU  
MANUSIA NORMAL DAN KANSER**

**ABSTRAK**

Penggunaan nanopartikel perak (AgNPs) yang disintesis daripada tumbuhan semakin meningkat dalam pelbagai industri, termasuk sektor farmaseutikal dan makanan. Penggunaan yang meluas ini telah menimbulkan kebimbangan mengenai profil keselamatannya. Kajian ini bertujuan untuk mengkaji kesan toksik dan mekanisme nanopartikel perak biogenik (AgNPs-GA) yang disintesis menggunakan ekstrak daun *Garcinia atroviridis* ke atas sel kanser paru-paru manusia (A549) dan sel paru-paru normal (BEAS-2B) secara *in vitro*. Toksisiti dinilai menggunakan ujian MTT untuk menentukan nilai IC<sub>50</sub> AgNPs-GA di dalam kedua-dua jenis sel. Nilai IC<sub>50</sub> ini digunakan untuk merawat sel-sel yang berkenaan bagi menilai penghasilan reaktif oksigen spesies (ROS), apoptosis, kerosakan DNA, kepekatan ion perak, dan penyerapan selular melalui ujian CM-H<sub>2</sub>DCFDA, pewarnaan berganda DAPI dan AOPI, assai komet, ICP-OES, dan TEM. Ekspresi mRNA dan profil metabolik dinilai menggunakan PCR masa nyata secara kuantitatif dan metabolomik tak bersasar menggunakan kromatografi cecair prestasi tinggi ultra-spektrometri jisim Orbitrap (UHPLC-Orbitrap-MS). Hasil kajian menunjukkan bahawa AgNPs-GA merencat pertumbuhan sebanyak 50 % di dalam sel A549 dan BEAS-2B, dengan nilai IC<sub>50</sub> masing-masing antara 20–28 µg/ml dan 12–35 µg/ml. Nilai indeks selektif (SI) bagi AgNPs-GA adalah di bawah 3, mengklasifikasikannya sebagai agen sitotoksik tidak selektif, kerana ia telah mengaruh keseluruhan ketoksikan kepada kedua-dua jenis sel kanser dan bukan kanser. AgNPs-GA diserap dan disimpan di dalam lisosom, nukleus

dan mitokondria, menyebabkan peningkatan pelepasan ion perak ( $\text{Ag}^+$ ) ke dalam kedua-dua sel. Kedua-dua titisan sel menunjukkan peningkatan aras ROS selular dan kerosakan DNA yang serius. Terdapat peningkatan yang ketara dalam tahap ekspresi mRNA *ATM*, *Ku80*, dan *DNA-PKcs* dalam kedua-dua titisan sel. Sementara itu, ekspresi mRNA *RAD51* didapati menurun di dalam sel A549 tetapi meningkat di dalam sel BEAS-2B. Melalui analisis pemprofilan metabolomik, AgNPs-GA didapati mengganggu laluan isyarat yang berkaitan dengan metabolisme glutation, nukleotida, dan tenaga di dalam kedua-dua jenis sel, dan ini telah menyebabkan pengekspresan yang berbeza kepada metabolit L-glutation, xantina, dan  $\text{NAD}^+$  selepas rawatan. Laluan-laluan ini diketahui berkait rapat dengan tekanan oksidatif dan kerosakan DNA, yang akhirnya menyebabkan kematian sel secara apoptosis. Ini seterusnya mengesahkan bahawa AgNPs-GA mempunyai kesan sitotoksik di dalam kedua-dua jenis sel kanser dan normal manusia pada kepekatan yang diuji dalam kajian ini. Kesimpulannya, penemuan ini memperlihatkan potensi risiko yang berkaitan dengan pendedahan kepada AgNPs-GA, dan ini menunjukkan kepentingan terhadap pertimbangan yang teliti, terutamanya untuk aplikasi bioperubatan dan terapeutik. Penemuan ini boleh digunakan sebagai bahan bukti berasaskan kajian *in vitro* untuk menyokong pembangunan dasar berkaitan dengan pencirian keselamatan AgNPs biogenik pada masa hadapan.

**CHARACTERISATION OF BIOGENIC SILVER NANOPARTICLES-  
GARCINIA ATROVIRIDIS TOXICOLOGICAL EFFECTS IN NORMAL AND  
CANCER HUMAN LUNG CELLS**

**ABSTRACT**

Silver nanoparticles (AgNPs) synthesized from plants are increasingly used across various industries, including the pharmaceutical and food sectors. This widespread use has raised concerns about their safety profiles. This study aimed to examine the toxic effects and mechanisms of biogenic silver nanoparticles (AgNPs-GA) synthesized using *Garcinia atroviridis* leaf extract on human lung cancer cells (A549) and normal lung cells (BEAS-2B) *in vitro*. Cytotoxicity was evaluated using the MTT assay to determine the IC<sub>50</sub> values of AgNPs-GA in both cell types. The IC<sub>50</sub> values were applied to treat the respective cells for evaluating reactive oxygen species (ROS) production, apoptosis, DNA damage, silver ion levels, and cellular uptake using CM-H2DCFDA assay, DAPI and AOPI double staining, comet assay, ICP-OES, and TEM, respectively. The mRNA expression and metabolic profiles were further assessed using quantitative real-time PCR and untargeted metabolomics based on ultra-high-performance liquid chromatography-Orbitrap mass spectrometry (UHPLC-Orbitrap-MS), respectively. The results showed that AgNPs-GA inhibited 50% of the growth in A549 and BEAS-2B cells, with IC<sub>50</sub> values ranging from 20–28 µg/ml and 12–35 µg/ml, respectively. The selective index (SI) values of AgNPs-GA were below 3, classifying it as a non-selective cytotoxic agent, as it induced general toxicity in both cancerous and non-cancerous cell types. AgNPs-GA were primarily internalized and deposited within lysosomes, nucleus, and mitochondria, leading to an increased release of ionic silver (Ag<sup>+</sup>) inside both cells. Both cell lines showed elevated cellular

ROS levels and severe DNA damage. A marked increase of *ATM*, *Ku80*, and *DNA-PKcs* mRNA levels was observed in both cell lines. Meanwhile, *RAD51* mRNA expression was downregulated in A549 cells but upregulated in BEAS-2B cells. Through metabolomic profiling analysis, AgNPs-GA was found to disrupt signalling pathways associated with glutathione, nucleotide and energy metabolism in both cell types, leading to differential expression of L-glutathione, xanthine and NAD<sup>+</sup> metabolites after treatment. These pathways are known to be associated with oxidative stress and DNA damage, that ultimately causes apoptotic cell death. This further confirms that AgNPs-GA exhibited cytotoxic effect in both human lung cancer and normal cells at the concentration tested in this study. These findings highlight the potential risks associated with AgNPs-GA exposure and underscore the importance of careful considerations particularly for biomedical and therapeutic applications. These findings may serve as evidence based on *in vitro* studies to support the establishment of future policies regarding the safety profile of biogenic AgNPs.

# CHAPTER 1

## INTRODUCTION

### 1.1 Research background

Nanotechnology is a broad area of study that involves the application of various materials at the scale of 1 to 100 nanometers ( $1\text{ nm}=10^{-9}\text{ m}$ ), known as nanoparticles (Chandra et al., 2020). This technology is extensively applied in translational research. Nanoparticles hold immense potential for improving the efficiency of various medical procedures such as delivering drugs (Malik et al., 2022). Metallic nanoparticles (MNPs) are commonly used in biomedical sciences and engineering within the field of nanotechnology. Chandra et al., (2020) found that MNPs have been used for targeted drug delivery and magnetic resonance imaging (MRI). Besides, MNPs are an excellent contender for wound dressing materials and ideal materials for biosensor interface design (Cruz et al., 2020). The high surface-to-volume ratio and reactivity of MNPs can influence their potential in various medical applications (Cruz et al., 2020). These properties allow MNPs to interact more effectively with biological systems, improving their efficacy in drug delivery to specific cells or tissues, enhance imaging techniques, and develop sensitive diagnostic tests (Cruz et al., 2020). Among the inorganic metal-based nanoparticles, silver nanoparticles (AgNPs) are particularly notable for their attractive physicochemical properties and biological activities.

There are various methods can be implemented to produce AgNPs, such as biological, chemical, and physical processes (Chandra et al., 2020; Zhang et al., 2020). There are two main methods used for the production of inorganic nanoparticles: the top-down and the bottom-up approaches (Zhang et al., 2020). The former involves breaking down the bulk materials into tiny structures in nanosized, which is often accomplished through mechanical processes, chemical, or

physical (Alharbi et al., 2022). The bottom-up approach, on the other hand, involves using biological or chemical resources to create basic units such as atoms and molecules to build up nanoparticles (Vigneswari et al., 2021).

Various biological systems, such as plants (Varadharaj et al., 2019), fungi (Skanda et al., 2022), bacteria (Truong et al., 2022), seaweed (Deepak et al., 2018), lichen (Goga et al., 2021) and algae (Chugh et al., 2021) have been studied to produce AgNPs. These include small biomolecules such as amino acids, carbohydrates, and enzymes (Vigneswari et al., 2021; Malik et al., 2022).

According to a study conducted by Chandrakala and colleagues, (2022), AgNPs can be utilized as a part of a strategy to deliver vaccines, nucleotides, and conventional medications. Furthermore, AgNPs are widely used in a wide range of products, such as humidifier, water filtration systems and toothpaste, due to their antimicrobial properties (Zhang et al., 2020). According to the study conducted by Zhang et al., (2020), AgNPs produced by plants are effective against various types of Gram-positive and Gram-negative agricultural pathogens. In addition to these abovementioned properties, the researchers noted that AgNPs exhibited antitumorigenic properties by inducing cytotoxicity against different leukaemia cell lines (Mostafavi et al., 2022). For instance, AgNPs produced by the plant extract of *Catharanthus roseus* leaf exhibited anti-cancer effects by suppressing the growth, invasion and migration of HepG2 human liver cancer cells *in vitro* (Azhar et al., 2020).

Moreover, due to their wide variety of applications, the toxicity of AgNPs has become a subject of increasing attention, and researchers have recently studied their effects on human health and well-being. (Ferdous and Nemmar, 2020; Nie et al., 2023). In most cases, AgNPs exposure can be initiated through inhalation during various stages of the production and handling process (Li and Cummins, 2020). Numerous studies have shown that inhaled NPs are more toxic than their

larger counterparts (macro-scale) when it comes to respiratory toxicity. These findings suggest that the higher surface reactivity of these substances can trigger the development of respiratory toxicity (Zhao et al., 2021).

Malaysia is known for its rich supply of medicinal plants, which are regarded as the primary sources of substances used in pharmaceutical and therapeutic procedures (Bakar et al., 2018; Ali Alsarhan et al., 2021). *Garcinia atroviridis* (*G. atroviridis*) is one of the most frequent forms of medicinal plants discovered in Malaysia. The fruits and leaves are often used to cure a variety of ailments, including coughing and throat irritation, and pre- and postpartum medication (Al-Mansoub et al., 2014; Hamidon et al., 2017). Additionally, indigenous and Malay communities consume the leaves and fruits as a flavoring agent and in salad (Al-Mansoub et al., 2014; Zulkifli et al., 2020).

## **1.2 Problem statement**

For decades, the use of AgNPs has been widely explored in various fields, especially in pharmaceutical and biomedicine applications due to their unique pharmacological and physicochemical properties. In recent years, AgNPs have been widely used in wound healing (Kubavat et al., 2023) and bone graft procedures in dental sector (Narciso et al., 2021), due to their antimicrobial properties (Munhoz et al., 2023; Thomas and Thalla, 2023). AgNPs were discovered to have potential to be employed as biosensors for medical devices (Naqvi et al., 2023), drugs carriers (Shakeel et al., 2023), and as an effective treatment agent for cancer (Singh et al., 2023). Despite the various applications of AgNPs, the evaluation of their potential toxic effects is still a major concern for the environment and human health. Furthermore, underlying mechanisms responsible for the toxicological properties of AgNPs particularly derived from biosynthesised approaches are yet to be explored.

### **1.3 Objectives of the study**

#### **1.3.1 General objective**

This study aimed to investigate the underlying mechanism responsible for the toxicological effects of biogenic silver nanoparticles (AgNPs-GA) in both A549 cancerous and BEAS-2B non-cancerous human lung cell lines.

To achieve the above-mentioned objectives, several specific objectives have been conducted and measured in this study. The list of specific objectives were as follow:

#### **1.3.2 Specific objectives**

1. To biosynthesise AgNPs-GA from *Garcinia atriviris* leaves extract and characterise its physicochemical properties.
2. To evaluate the effects of AgNPs-GA on the growth inhibition, production of reactive oxygen species (ROS), silver ion ( $\text{Ag}^+$ ) release, mechanism of cellular uptake and cell death in both A549 and BEAS-2B cell lines.
3. To evaluate the effects of AgNPs-GA on genotoxic activity and mRNA expression of related DNA damage and repair pathways (*ATM*, *DNA-PKcs*, *RAD51*, and *Ku80*) in both A549 and BEAS-2B cells.
4. To investigate the effect of AgNPs-GA on metabolome profiles of A549 and BEAS-2B cells.

## CHAPTER 2

### LITERATURE REVIEW

#### 2.1 Lung

##### 2.1.1 Anatomy, histology, and physiology

The lungs are the major organs of the respiratory system and are categorised into sections or lobes. As shown in Figure 2.1, the right lung has three lobes (upper lobe, middle lobe, and lower lobe), while the left one only consists of two lobes (upper lobe and lower lobe). Each lobe is connected to a specific region of the bronchi (Homer and Britto, 2014). The structures of the lungs are composed of the respiratory bronchioles, the alveolar ducts, and the alveoli. These components are responsible for the exchange of gas (Mack et al., 2020).

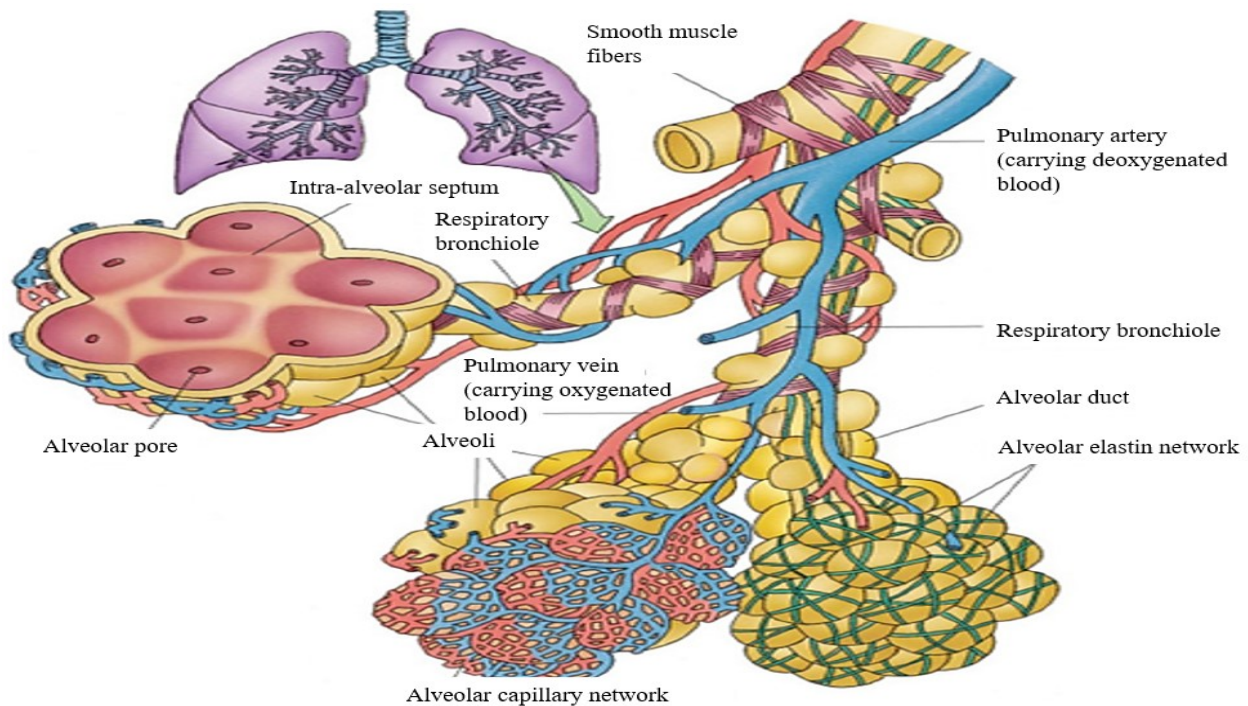


Figure 2.1 The lower respiratory system displays the relationship between the respiratory bronchioles, alveoli, and terminal bronchioles. Notice that the alveolar pores are connected to the alveoli. As the branch of the airways passes through the alveolar membrane, the smooth muscle fibers in the airways become shorter. Extracted from Homer and Britto, (2014).

The lungs have two vital functions. The first function is ventilation-perfusion, which helps to deliver oxygen to the body and to remove carbon dioxide. Meanwhile, the other one is host defense against harmful chemicals, particulates, and airborne pathogens. These two functions are interrelated (Albertine, 2015). The goal of the airways is to provide the alveoli with clean and fresh air. This is done through the filtration of air that contains pollutants and micro particles. It also eliminates pathogens and viruses (Arroyo and Schweickert, 2015). The lungs can be divided into two parts: the gas exchange and the conducting zones. The former part comprises the respiratory and terminal bronchioles, while the latter includes the trachea, alveolar duct, and the bronchi. The respiratory zone is composed of the alveoli, alveolar ducts, and the respiratory bronchioles (Figure 2.1) (Homer and Britto, 2014).

### **2.1.2 Pathophysiology**

Lung disease can be categorised into two main categories, which are obstructive and restrictive. Obstructive lung disease is characterised by impaired expiration. For instance, it can result in a reduction in the forced expiratory volume (FEV1) and forced vital capacity (FVC) (Haddad and Sharma, 2022). Some of the secondary types of obstructive disease include cystic fibrosis (CF) and non-cystic fibrosis bronchiectasis (NCFB) (Haddad and Sharma, 2022). Two main examples of this disease are chronic obstructive pulmonary disorder (COPD) and asthma (Haddad and Sharma, 2022). COPD is the primary lung pathophysiology whereby gastro oesophageal reflux (GOR) is a comorbidity in this disorder (Ward et al., 2018). Restrictive lung disease, on the other hand, is a type of lung disease that limits the lung's ability to expand. In terms of characteristics, restrictive lung disease can result in a decrease in the FEV1 and an increase in the FEV1/FVC. Some other conditions that can cause this type of lung disease include idiopathic pulmonary fibrosis, sarcoidosis, and pneumoconiosis (Haddad and Sharma, 2022).

### **2.1.3 Lung carcinogenesis**

The process of cancer development involves the transformation of normal cells into cancer cells. Lung cancer develops in the lungs through a process called carcinogenesis, which involves the accumulation of genetic mutations caused by factors such as smoking, environmental toxins, or genetic predisposition (Heng et al., 2021; Stading et al., 2021). These mutations disrupt normal cell regulation, leading to uncontrolled cell growth, resistance to apoptosis, and the eventual formation of malignant tumors that can invade surrounding tissues and metastasize (Hanahan, 2022). Exposure to tobacco smoke is one of the leading causes of lung carcinogenesis (Vinay et al., 2021; Tang et al., 2022). It has been reported that individuals who continue to smoke have a 20 to 50 times greater risk of developing lung cancer compared to non-smokers (Malhotra et al., 2016). The length of time a person smokes is acknowledged as the most critical factor affecting the development of this disease (Malhotra et al., 2016). While nicotine does not cause lung cancer, tar in cigarettes can lead to the development of this disease (Akhtar and Bansal, 2017). Approximately 3,500 compounds in tar are known to be carcinogenic to humans. Most of these compounds are classified as polycyclic aromatic hydrocarbons (PAHs), such as dibenzo[a,h]anthracene (DBA), benzo[a]pyrene (BP), and 3-methylcholanthrene (MC) (Stading et al., 2021; Vinay et al., 2021). Other known carcinogens include aza-renes, aromatic amines, aldehydes, and aromatic amines (Bracken-Clarke et al., 2021). Tar also contains various inorganic compounds, such as arsenic, chromium, hydrazine, and several others (Akhtar and Bansal, 2017). Prolonged exposure to these compounds results in DNA adducts, which lead to genetic abnormalities and mutations (Stading et al., 2021). The failure of DNA repair mechanisms in response to this damage leads to the development of cancer cells (Tang et al., 2022).

Nicotine is a significant component of tobacco smoke. Although it is known to be an addictive substance, nicotine is believed to be non-carcinogenic, as mentioned previously (Akhtar

and Bansal, 2017; Vinay et al., 2021). Nevertheless, nicotine can still cause cancer when it is converted to nitrosamine compounds, particularly nitrosamine ketone and nitrosornicotine (Bracken-Clarke et al., 2021; Vinay et al., 2021). According to Bracken-Clarke et al., (2021) the use of nitrosamines can increase DNA methylation, which is believed to contribute to the development, survival, and invasion of cancer cells. It also increases the activity of the nicotinic acetylcholine receptor. The lack of evidence supporting the carcinogenic properties of nicotine has led to the development of devices that deliver this substance without the burning of tobacco. Some of these include electronic cigarettes and nicotine patches (Tang et al., 2022). The electronic cigarettes (e-cigarettes) and vaping fluids which are commonly used nowadays contain various carcinogens. Some of these include nitrosamine ketone, organometal compounds, PAHs, and aldehyde (Bracken-Clarke et al., 2021). e-cigarette nicotine can be nitrosated, producing nitrosamines and thereby causing two carcinogenic effects, namely DNA damage induction and DNA repair inhibition. It was also reported in a study that e-cigarette aerosol can cause carcinogenic in mice (Tang et al., 2022).

Besides tobacco smoking, lung cancer can also be attributed by other factors, such as air pollution from vehicles and on-the-job exposure to toxic chemicals. The hazardous substances from outdoor air pollution include carbon monoxide, nitrogen oxide, and ozone (Loiselle et al., 2019). Meanwhile, various types of chemical compounds from different types of industrial and occupational activities, such as radon, chromium, arsenic, and lead, have been linked to lung cancer (Loiselle et al., 2019). Poorly ventilated indoor spaces can expose individuals to radon, a radioactive gas that seeps from soil, rock, and construction materials into buildings (Akhtar and Bansal, 2017). Radon decays into radioactive particles that, when inhaled, emit alpha radiation, damage lung tissue, and increase the risk of lung cancer, particularly with long-term exposure

(Yoon et al., 2016). Besides coal burning, other sources of indoor air pollution include fireplaces and wood burning stoves within poorly ventilated houses release the particulate matter and carcinogenic compound like PAHs (Malhotra et al., 2016). These chemicals are known to induce cancer by causing the production of reactive nitrogen (NOS) and oxygen species (ROS), leading to DNA damage, chronic inflammation, chromosomal alterations, and effects on the cell cycle and its proteins. These genetic alterations can lead to the development of cancer (Akhtar and Bansal, 2017; Vinay et al., 2021).

Numerous studies have identified family history as a major risk factor for lung cancer. According to a study conducted by the International Lung Cancer Consortium, individuals with a first-degree relative (mother, father, and sibling) suffering from the disease have 1.5 times higher risk of developing lung cancer than those otherwise (Akhtar and Bansal, 2017). In another study, the presence of single-nucleotide polymorphic variants (SNPs) and mutations in the genetic code (15q25, 5p15, and 6p21 regions) were found to be associated with the development of lung cancer (Malhotra et al., 2016). Additionally, high consumption of alcohol, unhealthy diets, and obesity are known to increase the risk of developing lung cancer, and people who have respiratory conditions, such as tuberculosis and COPD, are more prone to developing the disease (Malhotra et al., 2016; Akhtar and Bansal, 2017). Exposure to ionising radiation (Malhotra et al., 2016) and Epstein-Barr virus, HIV, and human papillomavirus (HPV) infections have also been linked to lung cancer (Akhtar and Bansal, 2017).

Generally, there are two types of lung cancer: 1) small-cell lung cancer (SCLC) and 2) non-small cell lung cancer (NSCLC). These two types are the main contributors for most of the lung cancer cases, which derived from epithelial cells of lung (Centers for Disease Control and Prevention (CDC), 2023). Approximately 15 % of lung cancer cases are attributed to SCLC, while,

around 85 % of the cases are NSCLC (Basumalik and Agarwal, 2022). Compared to SCLC, NSCLC is less aggressive and more common. SCLC is more likely to spread to other organs and therefore, it is regarded as a highly malignant tumour that is mainly caused by the neuroendocrine cells. In 2016, a study conducted by Siang et al. revealed that secondary lung cancer occurs when the primary lung cancer cells metastases to other parts of the body, such as the bone, breast, and colon (Siang and John, 2016) .

The major classifications of NSCLC include adenocarcinoma, large cell carcinoma, and squamous cell carcinoma (SCC). It was estimated that 40 % of all lung cancers are attributed to adenocarcinoma (Sánchez-Ortega et al., 2021). Adenocarcinoma, which starts in the glands located outside the lung, is most commonly found in people who are under 45 years old, women and non-smokers (Jain et al., 2021). Another type of lung disease, SCC, is mainly attributed to individuals who have a history of smoking, i.e. within 25 to 30 % (Jain et al., 2021). The three main types of SCC are basaloid, keratinising, and non-keratising (Kadota et al., 2015). These tumours usually appear in the central part of the lung and can form cavities when they grow excessively (Xie et al., 2022). A study by Jain et al., (2021) found that men are more likely to develop NSCLC than women. This can be attributed with typically higher smoking rates in men, increased exposure to carcinogens like radon, asbestos, and other chemicals in certain occupations, hormonal factors such as the protective role of estrogen in women, and men's tendency to seek medical check-up less frequently, resulting in delayed diagnoses (Jemal et al., 2018). In most cases, the cancer starts in the larger bronchi of the lungs (Sánchez-Ortega et al., 2021). Approximately 10-15% of the cases are classified as large cell carcinoma, which is the rarest of all lung cancers. This type of cancer usually develops rapidly in one area of the body and is often difficult to detect until it has spread (Sánchez-Ortega et al., 2021). Almost 70 % of all surgical cases are caused by

adenocarcinoma which accounts for 60% of all NSCLC cases (Gridelli et al., 2015). This malignant epithelial tumor is typically characterized by glandular differentiation and mucin production (Xie et al., 2022). The WHO classified all types of adenocarcinomas into four subclasses: micropapillary, solid, invasive, and colloid (Kadota et al., 2015). A 2017 review found that exposure to low molecular weight polycyclic aromatic hydrocarbons at 50 ng per cigarette from tobacco smoking can lead to SCLC, while exposure of peripheral lung tissue to nitrosamines at 110 ng per cigarette in tobacco smoke can result in adenocarcinoma (Akhtar and Bansal, 2017).

Apart from its histological characteristics, lung cancer can also be classified based on molecular subtype. In recent years, the number of targeted genes used as biomarkers for both diagnosing and predicting the prognosis of the disease has increased. These include B-Raf proto-oncogene (BRAF) mutation, human epidermal growth factor receptor-2 (HER2) mutations, ErbB2 receptor tyrosine kinase-2 (ERBB2) and RET proto-oncogene (RET) fusion (Rajadurai et al., 2019). BRAF is a gene that encodes a protein involved in the MAPK/ERK signalling pathway, which regulates cell growth (Riudavets et al., 2022). Mutations in the BRAF gene, particularly the BRAF V600E mutation, have been identified in a subset of NSCLC patients (Guaitoli et al., 2023). Detection of this mutation can help guide the use of targeted therapies, such as BRAF inhibitors, which have shown efficacy in treating cancers driven by this mutation (O’Leary et al., 2019; Perrone et al., 2022). Another example emphasizing the importance of biomarkers, such as programmed cell death ligand-1 (PD-L1), is its ability to predict favorable outcomes in lung cancer treatment (Rajadurai et al., 2019). According to Rajadurai et al., (2019), patients with advanced cancer who display high levels of PD-L1 expression are more likely to achieved better treatment outcomes.

Lung cancer in non-smokers differs from that in smokers in terms of the molecular characteristics of the cancer cells (Kuśnierczyk, 2023). According to Akhbar and Bansal, the mutation rates in EGFR, HER2, EML4-ALK, RET, and ROS1 genes, were significantly higher in non-smokers compared to tobacco smokers, who showed a higher mutation rate in the K-RAS gene (Akhtar and Bansal, 2017). The mutation rates in these gene variants among non-smokers suggest that lung cancer in this group may develop through distinct molecular pathway. These gene variants are often associated with oncogenic drivers – mutations that directly contribute to cancer development by promoting uncontrolled cell growth. For example, mutations in EGFR (epidermal growth factor receptor) is common in non-smokers and can be targeted by specific therapies (Khaddour et al., 2021). In contrast, K-RAS mutations are more frequently observed in smokers, often linked to tobacco-related carcinogenesis, which involves the accumulation of DNA damage from carcinogens in cigarette smoke (Caliri et al., 2021; Wang, 2021). These findings highlight the importance of personalized treatment strategies, as the molecular profiles of lung cancer in smokers versus non-smokers, and those influenced by epigenetic factors differ significantly, affecting treatment options and outcomes.

## **2.2 Cellular Metabolism**

### **2.2.1 Fundamentals of cell metabolism**

Cell metabolism refers to the complex network of chemical reactions that occur within living cells to sustain life. These biochemical processes enable cells to obtain energy, synthesise necessary molecules, grow, reproduce, and respond to their environment (Zhu and Thompson, 2019). Metabolism can be divided into two categories, namely catabolism and anabolism. Catabolism can be defined as the breakdown of complex molecules into simpler ones, releasing energy that the cell can use for various activities. Anabolism can be defined as the synthesis of complex molecules from simpler ones, which requires energy input and is used for building cellular components like proteins, nucleic acids, and lipids. Through these metabolic pathways, cells convert nutrients into usable forms of energy (like ATP), produce building blocks for macromolecules, regulate cellular activities, and eliminate waste products (Davis and Rosenbaum, 2020).

Cellular metabolism plays a crucial role in carcinogenesis, as cancer cells often undergo metabolic reprogramming to meet the increased energy and biosynthetic demands required for rapid growth and proliferation. Key pathways, such as glycolysis (Warburg effect), the tricarboxylic acid (TCA) cycle, and oxidative phosphorylation, are frequently altered in cancer cells, enabling them to sustain growth and resist cell death, thereby contributing to tumor development and progression (Vanhove et al., 2019). In general, normal cells rely on oxidative phosphorylation in the mitochondria as their primary energy production mechanism, as it is highly efficient at generating large amounts of ATP (Figure 2.2A) (D'Alessandro and Zolla, 2012).

However, cancer cells preferentially rely on aerobic glycolysis for ATP production, rather than the oxidative phosphorylation pathway, a phenomenon known as the Warburg effect (Lebelo

et al., 2019). In the Warburg effect, cancer cells convert glucose into lactate (Figure 2.2B). This pathway produces significantly less ATP per glucose molecule compared to oxidative phosphorylation. However, this metabolic shift allows cancer cells to meet the high demand for biosynthetic precursors required for rapid cell growth and proliferation. This altered metabolism also facilitates cancer cells survive and thrive in the typically hypoxic (low oxygen) and acidic (low pH) environments found in cancers (Boedtkjer and Pedersen, 2020; Blaszcak and Swietach, 2021).

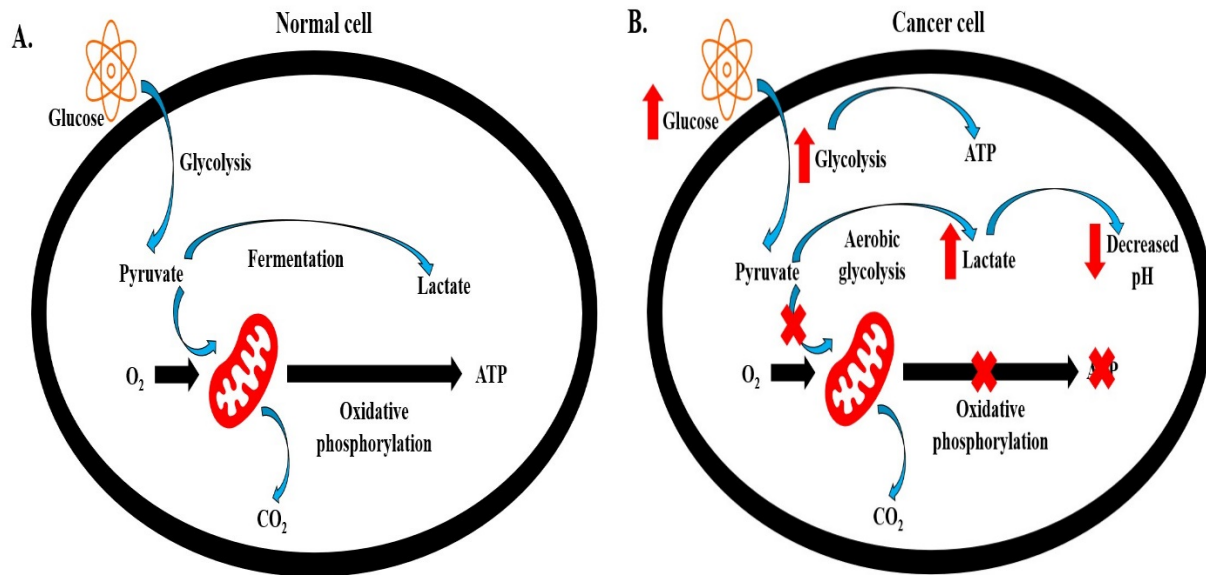


Figure 2.2 Normal and cancer cells metabolism. (A) Metabolism in a normal cell; increased flux of pyruvate into mitochondria for the generation of ATP; (B) Warburg Effect in the cancer cell; comprised of three main aspects: 1) enhanced glucose uptake 2) increased lactate secretion and 3) decreased oxidative metabolism (adapted from D'Alessandro and Zolla, 2012).

### 2.2.2 The hallmark of cancer metabolism

The term "cancer metabolism hallmark" refers to the specific changes in metabolism observed in cancer cells compared to normal cells. These alterations play a vital role in supporting the growth and survival of the cancer cells. Figure 2.3 illustrates the synthesis process of nucleotides, proteins, and lipids in cancer cells that are derived from amino acids, glucose, and glutamine. The proliferating cells require glucose, which is then converted to pyruvate through glycolysis. The PI3k/Akt pathway is a part of the glycolytic intermediates flow that controls the retention and import of glucose. The Krebs cycle begins with the pyruvate-to-acetyl-CoA conversion. MYC also regulates the catabolism and uptake of glutamine, which ensures the adequacy of  $\alpha$ -ketoglutarate ( $\alpha$ -KG) to fuel the TCA cycle and nitrogen for nucleotide synthesis (Finley et al., 2013). Glucose can also be used as a carbon source in the pentose phosphate pathway (PPP) to produce ribose-5-phosphate, which is converted into nucleotides (RNA and DNA) (Liu et al., 2019). Serine and glycine metabolism can also contribute to the pool of one-carbon metabolites that aid in nucleotide biosynthesis. Citrate is recycled to the cytosol for use in lipid synthesis. Lactate (primarily from glycolysis) and ammonia (from catabolism to amino acids) are secreted as waste (Finley et al., 2013; Vanhove et al., 2019).

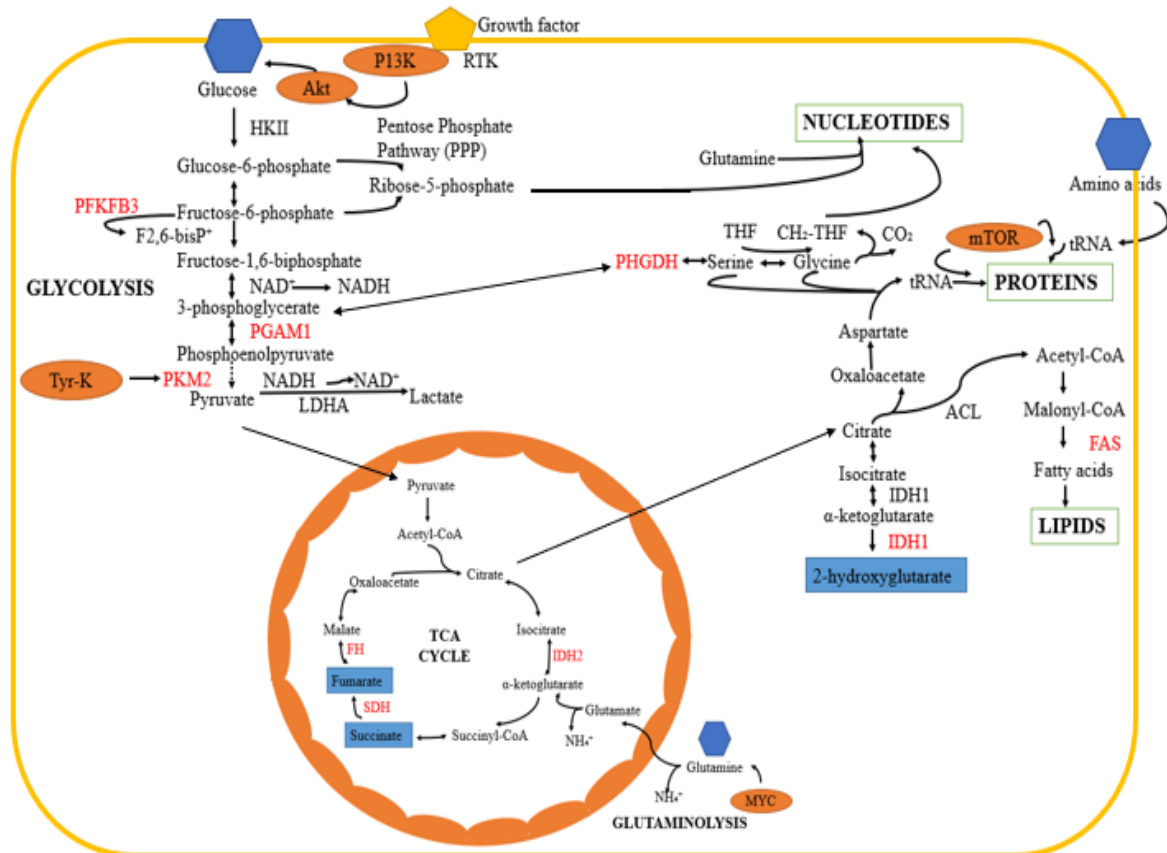


Figure 2.3 Cancer metabolism pathways (adapted from Finley et al., 2013); Highly proliferative cancer cell metabolism utilizes numerous pathways to generate energy, nucleotides, lipids, and amino acids. Signalling pathways controlling nutrient uptake and most common oncogenic events (shown in orange), metabolic enzymes (highlighted in red) and metabolites (shown in blue) whose levels, expression, or activity are altered in cancer, including tRNA.

The hallmarks of cancer include characteristics that allow cancer cells to grow uncontrollably and evade normal physiological processes (Hanahan, 2022). One of the emerging hallmarks is metabolic reprogramming. Through metabolic reprogramming, cancer cells modify their normal metabolic pathways to meet the increased energy, biosynthetic, and redox demands required for rapid growth and survival. Cancer cells often produce energy through a process called aerobic glycolysis, even when oxygen is available. This is different from normal cells, which usually use oxidative phosphorylation. (Lebelo et al., 2019). As above-mentioned, this shift allows

cancer cells to generate ATP quickly and produce the necessary building blocks for macromolecules like nucleotides, lipids, and proteins, as well as maintain redox balance, supporting their aggressive proliferation and ability to evade normal cellular controls (Lebelo et al., 2019).

Sustaining proliferative signalling, enabling replicative immortality, activating invasion and metastasis, evading growth suppressors, tumour-promoting inflammation, resisting cell death, avoiding immune destruction, inducing angiogenesis, genome instability and deregulating cellular energetics and mutation are hallmarks driven by metabolic reprogramming (Hanahan, 2022). Thus, this metabolic shift fuels key cancer hallmarks, and targeting these reprogrammed metabolic processes offers significant potential for the development of more effective cancer therapies.

## **2.3 Silver nanoparticles (AgNPs)**

### **2.3.1 Introduction**

Silver nanoparticles (AgNPs) is among the most widely used materials in nanotechnology-based nanostructures (Abass Sofi et al., 2022). They are composed of simple silver with an

estimated diameter from 1 to 100 nm, which are characterised by their high specific surface area, catalytic performance, surface energy, and excellent surface plasmon resonance (Ijaz et al., 2022). Compared to ordinary silver (bulk state), AgNPs perform better in terms of anti-bacterial and non-drug resistance properties (Thomas and Thalla, 2023) . They also have better anti-cancer characteristics (Alharbi et al., 2022; Garg et al., 2022). Due to their immense potential, the scientific community begins focusing on the development of AgNPs by utilising various processing methods, including biological, chemical, and physical routes.

### **2.3.2 Synthesis of AgNPs**

Most of the time, the synthesis of AgNPs is carried out using top-down and bottom-up methods, as shown in Figure 2.4. In the former method, the size of Ag metal is reduced physically by using tools and milled down to the nano level. On the other hand, the latter is a biological or chemical method that involves the creation of larger particles by the assembly of molecules or atoms (Garg et al., 2022; Hasan et al., 2022). In this process, the reducing agent is used to dissolve Ag salt into solvent, which then allows the silver to be reduced into Ag nanoparticles. This process prevents the aggregation of Ag nanoparticles (Ijaz et al., 2022).

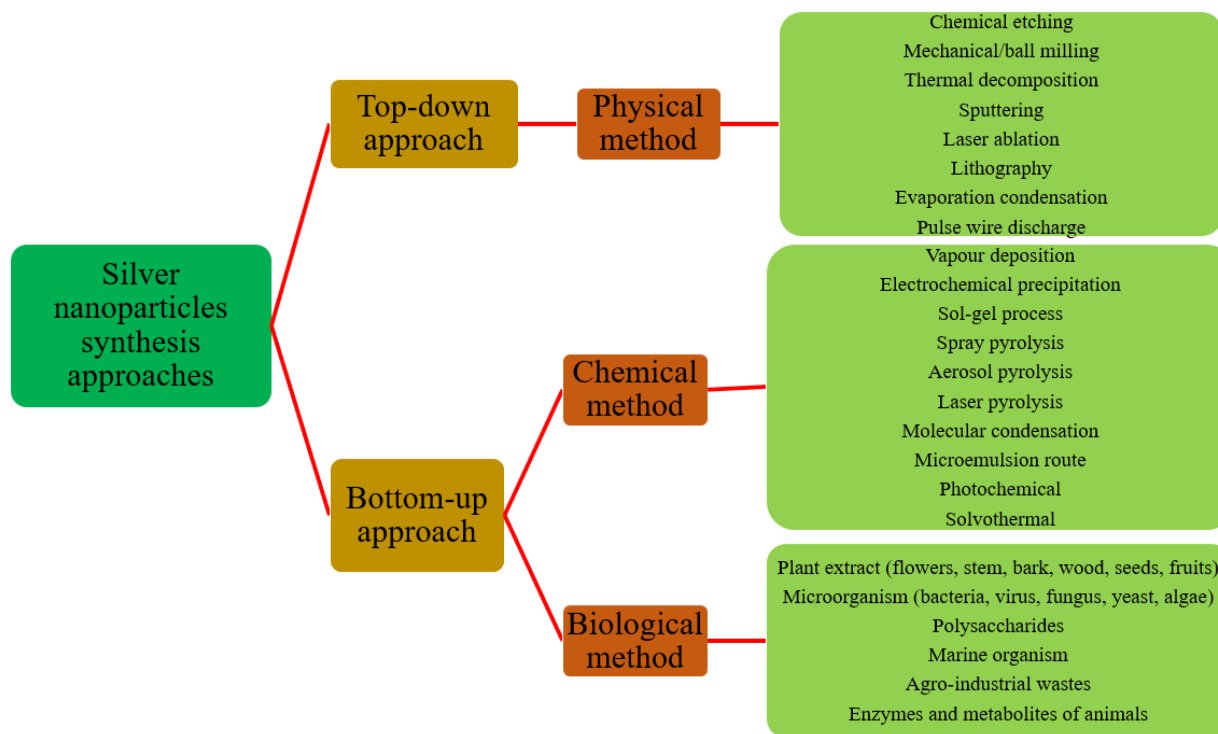


Figure 2.4 Different approaches to synthesized AgNPs (adapted and from Garg et al., 2022; Hasan et al., 2022)

Various physical methods, such as laser ablation, lithography, and evaporation-condensation, are commonly used to prepare AgNPs. The advantages of these methods include quick synthesis and the absence of harmful reagents (Alharbi et al., 2022; Nie et al., 2023). However, there are several drawbacks of these methods, such as solvent contamination, low yield, energy consumption, and non-uniform distribution (Alharbi et al., 2022), as well as the requirement for high concentrations (Nie et al., 2023).

Chemical reduction using organic and inorganic reducing agents is also commonly used to produce AgNPs. This method requires a reductant to convert  $\text{Ag}^+$  into AgNPs, such as block copolymers, ascorbic acid, citrate, and sodium borohydride (Nie et al., 2023; Shakeel et al., 2023). In turn, silver nitrate ( $\text{AgNO}_3$ ) can be utilised as a precursor (Alharbi et al., 2022). The chemical reduction method has several advantages over the physical methods, such as time efficiency and the ability to produce high yields of nanoparticles (Alharbi et al., 2022; Nie et al., 2023).

Unfortunately, the chemical substances involved in the production of AgNPs, such as citrate, are often harmful and costly (Alharbi et al., 2022). Furthermore, compared to other methods, chemical reduction is more challenging when it comes to producing AgNPs with a well-defined size. It requires additional steps to prevent particle aggregation (Nie et al., 2023). However, considering its advantages and simple operations, chemical reduction is still considerably a preferred method for producing AgNPs.

Considering the disadvantages of the chemical and physical synthesis processes of the nanomaterials, there has been a growing demand for more eco-friendly methods. With the key component of nanotechnology, the process of green synthesis of AgNPs is undergoing a progressive transformation. Various biological approaches were utilised for the synthesis of these nanomaterials, including plant extracts from leaves, flowers, roots, barks, and heartwood (Hasan et al., 2022; Medeiros et al., 2022; Kaithal et al., 2023), bacteria (Chauhan et al., 2023; Munhoz et al., 2023), fungi (Skanda et al., 2022), algae (Hasan et al., 2022), biopolymer (Rajawat et al., 2023) (Rajawat et al., 2023), and chitosan (Shakeel et al., 2023). In recent years, various industrial wastes, such as seed shells (Thomas and Thalla, 2023), pameo peel (Barbhuiya et al., 2022), as well as rice husk and coffee husk (Hasan et al., 2022), were used to produce AgNPs. The process of producing these materials using microorganisms has been widely acknowledged due to their high protein content and promising yields. Yet, among the major drawbacks of this process are the difficulties of growth and culture maintenance (Alharbi et al., 2022). In addition, it also requires additional processes, such as isolation and identification of microorganism. Temperature control is also required (Hasan et al., 2022).

The synthesising process of AgNPs using plant extracts has several advantages over the other methods. It is more eco-friendly, easy to handle, and offers a variety of advantages, such as

low toxicity, time and cost-effectiveness, and energy efficiency (Alharbi et al., 2022). The plant-based approach also eliminates the risk of contamination during storage (Hasan et al., 2022). Various phytochemicals found in plants, such as polysaccharides, flavonoids, and lignins, are utilised in the process of synthesising AgNPs whereby these elements act as stabilising agents, reducing agents, and capping agents (Garg et al., 2022; Ijaz et al., 2022).

The process of producing AgNPs from biological materials is simple and can be done with the help of AgNO<sub>3</sub> and its biomolecule components. This interaction was employed in previous studies in various fields, as shown in Figure 2.5.

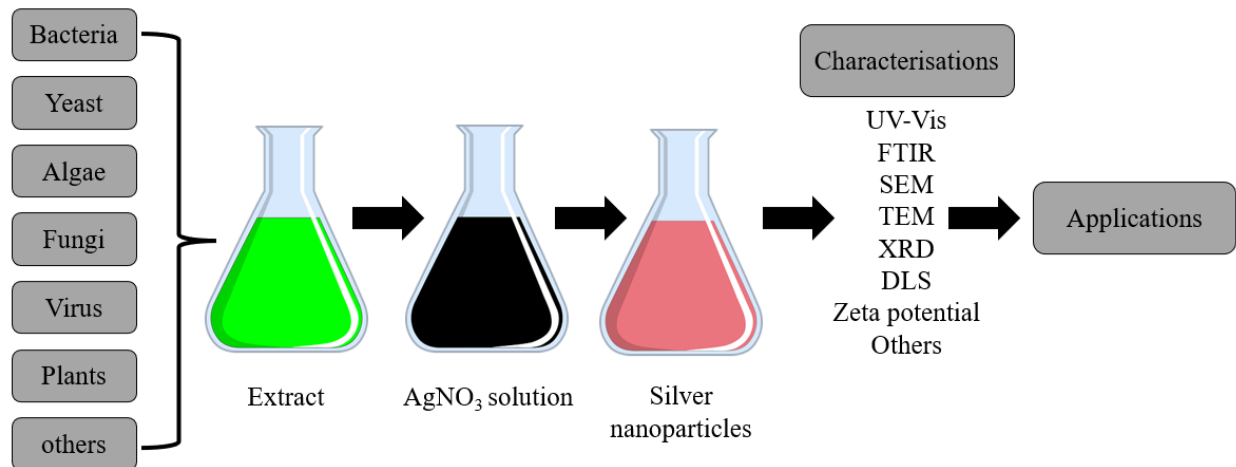


Figure 2.5 General green synthesis of silver nanoparticles (adapted from Alharbi et al., 2022; Ijaz et al., 2022)

The green synthesis process as shown in Figure 2.6 involves the formation of nanoparticles. They are mainly formed during three phases: the ion reduction reaction, the cluster formation, and the growth of the nanoparticles (Alharbi et al., 2022). In plant biomolecules, the presence of various hydroxy groups, including those found in polysaccharides, anthocyanins, amino acids, proteins, and flavonoids, can help to reduce and stabilise silver ions (Ag<sup>+</sup>) to Ag<sup>0</sup>. The reduction

to  $\text{Ag}^+$  triggers the creation of silver nuclei, leading to the production of AgNPs (Garg et al., 2022; Ijaz et al., 2022).

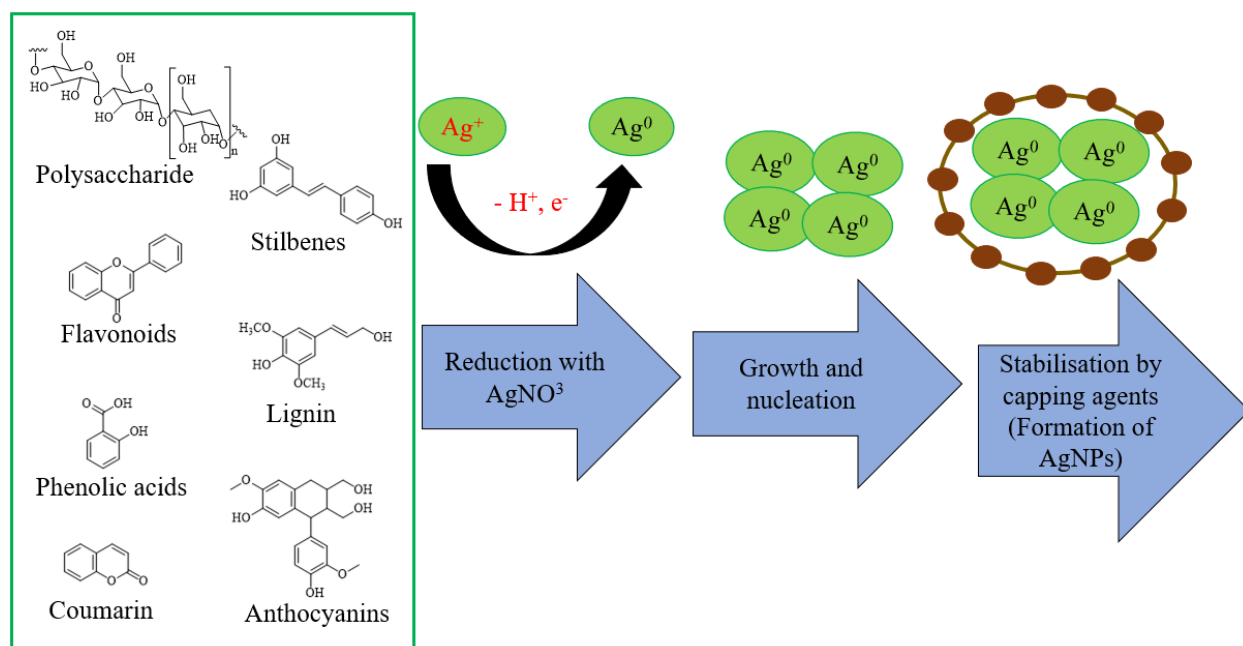


Figure 2.6 Representative mechanism for green synthesis of silver nanoparticles (adapted and modified from Alharbi et al., 2022; Garg et al., 2022; Ijaz et al., 2022)

The morphology and size of AgNPs are affected by various factors, such as the incubation period, light, temperature, pH, and the concentration of both  $\text{AgNO}_3$  and the extract (Alharbi et al., 2022). In their study, Alharbi et al., (2022) noted that the increase in the reaction temperature and the pH level can decrease the dimensions of the nanoparticles. According to their review, the increase in the plant extract's concentration can also increase the absorbance output, attributable to the fact that the longer the incubation period, the more AgNPs are produced. Additionally, the change in the reaction mixture's colour intensity (i.e. from yellow to brown), exhibited the AgNPs' formation. As anticipated in the study, while the reduction of  $\text{Ag}^+$  ions can be completed in a few minutes under sunlight, the reaction duration is longer under the dark. This is because the photons from direct sunlight can trigger the green process and promote the AgNPs' production. The AgNPs that were synthesised using different parameters exhibited a wide range of UV-Vis spectra (400-

500 nm) (Alharbi et al., 2022). Due to the varying environmental conditions during the green synthesis process, it is imperative to identify suitable biomolecular capping and stabilising agents that can be employed to form these nanoparticles.

The selection of solvent is crucial when extracting bioactive compounds from plant materials (Ijaz et al., 2022). Water is commonly used because it can dissolve a wide range of phytochemicals (Rahim et al., 2022; Al-Mashud et al., 2022; Khare et al., 2022; Kaithal et al., 2023; Singh et al., 2023). For instance, an aqueous extract of *Alstonia angustiloba* leaves has been used to synthesize silver nanoparticles, with alkaloids, flavonoids, and steroids acting as reducing agents (Rahim et al., 2022). Similarly, an aqueous extract of *Premna integrifolia* roots contains polyphenolic compounds, fatty acids, esters, ketones, flavonoids, and quercetin, which served as capping and stabilizing agents (Singh et al., 2023). The use of aqueous plant extracts is beneficial because it eliminates the need for toxic chemicals, making the synthesis process more environmentally friendly (Garg et al., 2022). In some cases, other solvents, such as ethanol or methanol, are employed, depending on the specific phytochemicals targeted and their solubility (Alharbi et al., 2022). For example, the methanolic extracts of *Madhuca longifolia* and *Pimenta dioica* leaves contain amino acids, alkaloids and polyphenols that reduce silver ions ( $\text{Ag}^+$ ) to silver nanoparticles (AgNPs) (Kaithal et al., 2023). Table 2.1 summarises the various synthesis approaches for the production of AgNPs.